## List of Corrections

# Mah Dissertat'n

Mark Pinese

December 13, 2014  Build 0.0.175

**ORIGINALITY STATEMENT**

‘I hereby declare that this submission is my own work and to the best of my knowledge it contains no materials previously published or written by another person, or substantial proportions of material which have been accepted for the award of any other degree or diploma at UNSW or any other educational institution, except where due acknowledgement is made in the thesis. Any contribution made to the research by others, with whom I have worked at UNSW or elsewhere, is explicitly acknowledged in the thesis. I also declare that the intellectual content of this thesis is the product of my own work, except to the extent that assistance from others in the project's design and conception or in style, presentation and linguistic expression is acknowledged.’

Signed …….....

Date …….....

# Acknowledgements

**Abstract**

Da abstract.

# Contents

# List of Figures

# List of Tables

# List of Algorithms

# Software versions

Unless otherwise specified, the following versions of software were used in all work.

| | |
|---|---|
| bamtools | 2.2.2 |
| bedtools | 2.18.2 |
| cd-hit | 4.6.1 **MP Fatal: plus patch** |
| FastQC | 0.10.1 |
| GATK | 3.1-1 |
| julia | 0.3.2 |
| MSigDB | 4.0 |
| muTect | 1.1.6-4-g69b7a37 |
| ncbi-blast | 2.2.29 |
| picard-tools | 1.109 |
| PROVEAN | 1.1.5 |
| Python | 2.7.8 / 3.4.1 |
| R | 3.1.1 |
| ahaz | 1.14 |
| depmixS4 | 1.3-2 |
| doParallelMC | 1.0.8 |
| Exact | 1.4 |
| GSVA | 1.14.1 |
| illuminaHumanv4.db | 1.24.0 |
| lumi | 2.18.0 |
| lumidat | 1.2.3 |
| nleqslv | 2.5 |
| NMF | 0.20.5 |
| nnls | 1.4 |
| org.Hs.eg.db | 3.0.0 |
| randomForest | 4.6-10 |
| Rsolnp | 1.14 |
| survival | 2.37-7 |
| samtools | 1.0 |
| SHRiMP | 2.2.3 |
| strelka | 1.0.14 |

| | |
|---|---|
| tabix | 1.0 |
| vcftools | 0.1.10 |
| VEP | 76 |

# Conventions

Unless otherwise specified, the following conventions are used throughout this dissertation.

- Indices in algorithm pseudocode are 1-based.
- Logarithms (log) and exponentiations (exp) are to base $e$.

# Chapter 1

# Signatures of Survival Processes in Pancreas Cancer

*Thesis: Specific molecular processes control survival of patients with resectable pancreatic ductal adenocarcinoma, and these processes can be identified using gene expression data.*

**Summary** Very little is known regarding the biological processes that control the survival of patients with pancreatic ductal adenocarcinoma (PDAC), the most common and aggressive form of pancreas cancer. As discussed in Chapter **??**, the wide range of relative patient survival times that is observed in practice is not well explained by extrinsic factors such as age at diagnosis, and perhaps instead reflects differences in the biological processes operating within each tumour. Recent molecular profiling work [4] has identified possible molecular subtypes within the previously homogenous group of PDAC, but these subtypes have not achieved the maturity or clinical application of those in breast cancer, and their discovery and validation has been hampered by ad-hoc methodology, and the lack of large, well-curated cohorts of PDAC samples. The recently-compiled APGI cohort contains the largest group of clinically annotated PDAC samples, with accompanying gene expression (GEX) and high-quality follow-up data, in the world. It presents a unique opportunity to apply modern techniques for prognostic signature identification to the discovery of biological processes that drive the clinical course of pancreas cancer. These signatures may find application as prognostic tools in their own right, but more importantly can supply much-needed information on the fundamental biology of the one common cancer that has, to date, been almost entirely refractory to all the tools of modern molecular medicine.

## 1.1 Introduction

Despite extensive research, PDAC remains a poorly-understood disease. Recent genomic profiling has revealed the genetic alterations that accompany the cancer [2], and a huge number of prognostic factors are known [10] (refer to chap:intro for further discussion on both points), but these findings have shed little light on the fundamental disease processes at work in individual tumours. This is a consequence of genetic and biomarker data being poorly-suited for understanding the biological state of a cell: although genetic alterations are central to the etiology of cancer, they give incomplete information on the pathways and systems actually active in a given tumour, and biomarkers supply non-causal readouts of cell state that are difficult to trace back to underlying biological processes.

Sitting between the regulatory function of transcription control, and the effector function of protein expression, GEX data integrate information from all aspects of cell condition, including genetic alterations, signalling pathway activity, and metabolic status. As such, it is unsurprising that GEX data are superior indicators of cell state, better than all other high-throughput measurement methods, such as protein expression or genetic alterations [18]. However, the involvement of GEX with so many biological inputs is also a weakness: typical differential expression studies will identify many hundreds of transcripts that vary between disease states, and the deconvolution of this complex set of hundreds of effects back to a small number of causative molecular processes remains challenging.

Historically, disease GEX profiling studies have largely refrained from attempting to infer the state of a few molecular processes from the many hundreds of differentially-expressed genes identified; notable early exceptions are for example [1, 13]. A number of factors are likely to have contributed to this reluctance: deconvolution methods require relatively large sets of high-quality measurements [16], early techniques were poorly-suited to the particular requirements of the GEX deconvolution problem, and the signature databases that assist the assignation of a biological annotation to the output from a deconvolution calculation (for example, the MSigDB [23]) are only now reaching maturity, with some areas of biology still underrepresented.

A simple synthetic example illustrates the problem and process of GEX deconvolution, and the character of solutions produced by both classical and modern techniques. Consider a group of samples, each of which is in one of three distinct biological states: state A, state B, and an intermediate state. Which state a sample is in affects the expression of two genes, gene 1, and gene 2: state A is associated with higher gene 2 expression than gene 1 expression; state B with higher gene 1 expression than gene 2; and the intermediate state with low expression for both genes (Figure 1.1). From the figure it is apparent that samples lie along two lines in transcription space; these lines I term metagenes.

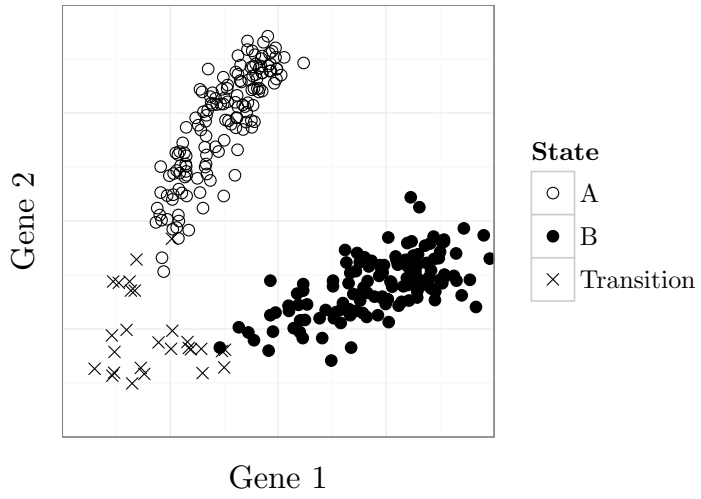


Figure 1.1: The gene deconvolution problem. Shown are the expression levels of two genes across three biological states, where each point represents the gene expression of a single sample in one of the three biological states. State A (hollow circles) is characterised by gene 2 > gene 1; state B (solid circles) by gene 1 > gene 2; and the intermediate state (crosses) by low levels of both genes. The challenge of gene deconvolution is to automatically infer, from unlabelled data (ie state is unknown), the dominant lines of gene expression (metagenes) along which most samples lie.

Accurately knowing the metagenes at work within a biological system considerably simplifies reasoning about transcription within the system. In the example of Figure 1.1, state A is simply associated with high metagene 1, state B with high metagene 2, and the transition state with low scores of both. Additionally, the loadings of genes on the metagenes themselves (the directions of the metagene arrows) provides information on transcriptional control within the system: metagenes define the axes along which cell state must move, and so provide a simpler and more accurate representation of cell state than the full set of gene expression measurements. Metagenes can also be considered to capture co-expressed modules of genes, with likely biological significance. The advantages of a metagene-centric perspective to interpreting GEX become increasingly apparent as more genes are considered, and when thousands of genes are measured per sample, deconvolving the highly complex patterns of expression of thousands of genes, to only tens of metagenes, represents a powerful reduction in complexity. However, in practical use deconvolution methods must operate in thousand dimensional spaces, rather than the two dimensions in this example, and the computational and methodological complexities involved, as well as the poor results yielded by traditional approaches, have limited the application of GEX deconvolution.

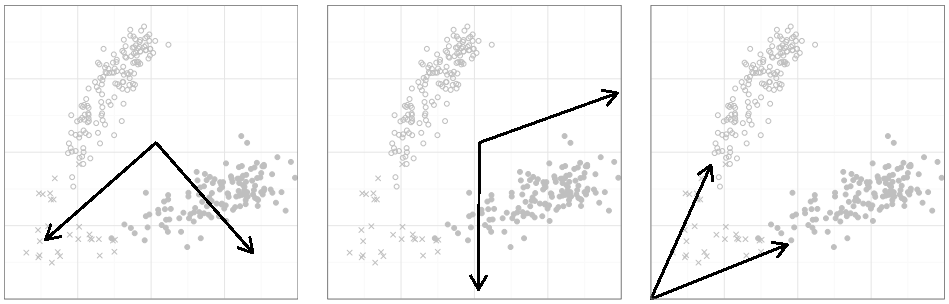

(a) PCA (b) ICA (c) NMF

Figure 1.2: NMF produces a more accurate GEX decomposition than either PCA or ICA. Metagenes found by each method are shown as arrows. PCA (panel a) produces metagenes that don't match the expression pattern seen in any sample; these metagenes do not have a ready biological interpretation. ICA (panel b) accurately identifies one metagene, but the inappropriateness of the non-Gaussianity criterion for these data leads to an incorrect estimate of the other; although this solution is better than that of PCA, not all metagenes align well with biology. NMF (panel c) provides the best deconvolution; the metagenes identified closely match the expression patterns observed, and reflect the true structure of co-expression within the samples.

A number of techniques from the field of matrix factorization have been applied to the GEX deconvolution problem, first principal component analysis (PCA) [1], then independent component analysis (ICA) [14], and more recently the various forms of non-negative matrix factorization (NMF) (first used for GEX in [3]). A number of reports have highlighted the unsuitability of PCA for GEX deconvolution, and the relative superiority of ICA [13, 19, 24]; this is primarily due to the PCA requirement that metagenes be orthogonal [15], a situation that is not supported by our knowledge of biology, and results in bizarre artefacts such as PCA metagenes not actually being aligned with the expression pattern of any sample (Figure 1.2(a)). Although the results from ICA are more interpretable than those from PCA, they still do not consider that GEX is a non-negative process: it is impossible to have a concentration of mRNA that is less than zero, and therefore for best interpretability we wish metagenes to have non-negative 'expression' as well. ICA does not produce solutions satisfying this requirement, and more importantly its non-Gaussianity objective is not necessarily optimal for GEX deconvolution (Figure 1.2(b)), reducing its ultimate utility. NMF techniques have the potential to produce excellent GEX decompositions (Figure 1.2(c)), but are relatively new methods that have very high computational requirements, and often require careful tuning, making their effective application challenging.

In addition to the general technical challenges of GEX deconvolution, is-

sues particular to pancreas cancer significantly complicate attempts to identify molecular processes at work within the tumours. Pancreas cancer is challenging to sample, and mRNA in the tissue degrades rapidly once extracted, complicating sample collection. Additionally, a feature of PDAC is the presence of a dense desmoplastic stromal reaction throughout the tumour, that is formed by genetically normal patient stroma cells [17]. The fraction of tumour cells that are actually cancerous varies by more than 10-fold between tumours [2], meaning that without careful correction, gene expression profiles are dominated by stromal cell fraction signals, and not true differential expression within a cell type. Microdissection has been used to separate cancer cells from surrounding stroma in order to simplify analysis [4], but current thought in the field is that the stroma in PDAC is an essential and enabling, if not in itself neoplastic, component of the tumour [17], and that the examination of cancer cell expression in isolation ignores the likely important interplay between the two major synergistic components of a tumour: transformed epithelial cells, and genetically normal stroma.

Due to these challenges to GEX deconvolution of PDAC, to date only one study (by Collisson *et al*, published in 2011) has reported a breakdown of PDAC GEX into a small number of biological modules [4]. This study examined microdissected cancer cells only, and found that the transformed epithelial cells of PDAC could be placed into three major categories, based on their patterns of gene expression. Tumours from these three categories followed distinct clinical courses, and cell lines exhibited category-specific sensitivity to therapeutic drugs. As the first report to identify potential clinically relevant molecular subtypes within PDAC, the Collisson study was a significant advance in the understanding of the molecular processes at play within what was previously considered a homogeneous disease. However, it also possesses shortcomings that limit its clinical utility.

Two main issues complicate the interpretation of the Collisson classes: microdissected cancer cells were used, and therefore stromal effects would be severely attenuated; and the deconvolution technique employed was tuned to achieve sample clustering, rather than GEX deconvolution. Consequently, although the Collisson classes could be a fundamental advance in the understanding of PDAC, they necessarily do not consider the full context of the disease, and potentially have artifically identified subgroups when in reality a smooth continuum of disease types may exist. Additionally, although the Collisson tumour subgroups were observed to follow different clinical courses, they were not explicitly generated to stratify patients by outcome, and so may not have captured the full biology underlying differential survival in PDAC.

A substantial gap remains in our molecular understanding of PDAC: little is known about the core molecular processes at work within both the cancer and stroma of different tumours, and almost nothing on those processes that control patient survival following diagnosis. Such a gap in knowledge is not merely of academic interest: a better understanding of the processes affect-

ing patient survival can lead directly to improved methods for staging, may stratify patients for customised therapies, and even suggest targets for therapeutics capable of transforming a poor-prognosis cancer into a good-prognosis one. The primary obstacle for the identification of these survival-associated processes in PDAC is one of data: a large, high-quality dataset of GEX measurements and associated well-curated clinico-pathological variables (CPVs) is needed. The APGI cohort addresses this data problem for the identification of fundamental survival processes in PDAC. As the largest cohort of PDAC samples, with accompanying GEX and curated CPVs, in the world, it can provide the data quality and cohort size required by modern GEX deconvolution techniques.

In this chapter I describe the application of NMF for the GEX deconvolution of genes associated with outcome. The metagenes thus identified represent orthogonal coordinately-expressed sets of genes which I then map to biological annotations, identifying the fundamental processes that may be involved in controlling the clinical course of a patient's pancreas cancer. The results of this work are directly applicable as signatures of survival time following diagnosis of PDAC, identify discrete biological processes that appear to determine outcome with pancreas cancer, and highlight fertile future avenues for research into this poorly-understood disease.

## 1.2 Results

Survival-associated metagenes were identified by selecting the set of genes which had GEX associated with outcome in the APGI cohort, and then performing NMF factorization to deconvolve the full matrix of gene expression signals into a small set of metagenes. Metagenes were found to fall into patterns defining two axes of outcome-associated cell state. These prognostic axes were then tested for association with clinical course and other CPVs, as well as known general prognostic signatures, and their prognostic ability was validated in a range of cancers by testing in separate cohorts. The two prognostic axes were then correlated with biological process signatures to associate axis scores with the activity of biological processes.

### Cohort characteristics and subsetting

228 unique patients from the APGI cohort had both GEX and follow-up data; for the discovery of metagenes specifically associated with PDAC survival these were subset to patients with histologically confirmed PDAC, who did not suffer perioperative mortality, and were treated within Australia. This subsetting produced a homogeneous 110-patient APGI discovery cohort, which was used for all metagene discovery work.

General characteristics of both the full APGI cohort, and the 110-patient PDAC APGI discovery cohort, are summarised in Table 1.1.

## Two axes predict survival with resectable pancreatic cancer in multiple cancers

**Probe selection** In order to focus the GEX deconvolution method on finding outcome-associated metagenes, it was necessary to filter the full set of gene expression data to only contain those genes that were likely to be associated with patient survival.

Unsupervised filtering to remove lowly-expressed and redundant probes yielded APGI cohort gene expression measurements for 13,000 genes, of which 361 were identified to be associated with time from diagnosis to disease-specific death (DSD) by sure independence screening (SIS)-feature aberration at survival times (FAST), using a complementary pair subset selection (CPSS) wrapper to reduce false positive rate. 50 variable selection runs on permuted data gave a median number of selected genes of 87.5, resulting in an estimated false-discovery rate (FDR) for the selection procedure of approximately 25%. This relatively high FDR was a consequence of the lenient selection parameters used, in an attempt to ensure that even genes for which expression was only weakly prognostic, were included.

**Prognostic genes factorized into six metagenes** NMF was used to reduce the complex expression patterns of 361 survival-associated genes into a small number of metagenes. NMF aims to approximate a non-negative gene $\times$ sample GEX matrix $A$ by a product of low-rank non-negative matrices $W$ and $H$, $A \approx WH$. The gene $\times$ metagene matrix $W$, termed the basis matrix, stores the contribution of each gene's expression to each metagene, whereas the metagene $\times$ sample matrix $H$, termed the coefficient matrix, contains the 'expression' of each metagene in each sample. The NMF procedure is highly sensitive to the choice of the rank of $W$ and $H$ (the number of metagenes) – a wrong rank will lead to metagenes either being incorrectly combined, or split.

The expression of the 361 survival-associated genes across the 110 patients of the APGI PDAC cohort was decomposed into metagenes by the sparse non-negative matrix factorization, long variant (SNMF/L) NMF algorithm. The number of metagenes (factorization rank) was automatically estimated to be 6, being the lowest rank for which the improvement in estimation error achieved by adding the next rank, was less than that observed for permuted data (Figure 1.3).

500 random restarts of rank 6 SNMF/L were then performed on the survival-associated gene matrix to yield the final factorization. The resultant clustering consensus matrix was stable (Figure 1.4), and the basis matrix $W$ was reasonably sparse (Figure 1.5). Sparsity of the basis matrix is a desirable condition for this analysis, as it indicates that metagenes are largely distinct transcriptional modules, with little overlap in terms of shared transcripts with high loadings; SNMF/L was selected against alternative NMF algorithms as its design favours solutions with sparse $W$. A table of values of

the basis matrix $W$ is available as app:sigs-w-matrix on page 31.

**Three metagenes together formed a prognostic model** The transcription patterns of genes associated with survival in the APGI cohort could be decomposed into just six largely distinct metagenes. Due to the presence of false positives in the 361 screened input genes, some of the metagenes will have no strong association with outcome. To identify which of the six metagenes were ultimately predictive of patient survival, I performed LASSO regression on the 110-patient APGI discovery cohort data, using non-negative least squares (NNLS)-estimated coefficients of each of the six metagenes as marginal predictors of outcome. The LASSO regularization parameter $\lambda$ was chosen by 10-fold cross-validation to be the highest value for which the mean test set partial likelihood deviance was within one standard error of the lowest mean value. This resulted in a final model in which three metagenes, MG1, MG2, and MG5, were selected as prognostic (Figure 1.6).

**Prognostic metagenes define two axes of cell transcription** Further investigation of the three prognostic metagenes revealed that they were associated: APGI patient coefficients for pairs MG1 and MG5, and MG2 and MG6 (the latter not selected by the LASSO), were mutually exclusive (Figure 1.7, Kendall's $\tau$ test $P < 1 \times 10^{-6}$ for each pair). This suggested that both metagenes in each pair captured the signal of a single axis of cell behaviour, with one measuring activation of the axis, and the other deactivation. For subsequent work I therefore combined the signals of the metagenes within each axis, to give axis activity summaries: Axis A1 activity = MG1 coefficient − MG5 coefficient; Axis A2 activity = MG6 coefficient − MG2 coefficient. Activation values for axes A1 and A2 were uncorrelated, indicating that these axes were orthogonal processes operating in the APGI cohort tumours (Figure 1.8, Kendall's $\tau$ test $P = 0.21$). Metagenes MG3 and MG4 also formed a mutually exclusive pair (not shown), but were not investigated further, as neither was determined to be prognostic by the metagene LASSO.

**The PARSE score** A repeat of the previous LASSO fit with 10-fold cross-validation (CV), this time using predictors of A1 activity, A2 activity, and the A1:A2 interaction, identified both A1 and A2, but not their interaction, as useful predictors of outcome. Coefficients from the LASSO fit were used to define a new risk score, the prognostic axis risk stratification estimate (PARSE), as PARSE score = $1.354 \times$ A1 activity + $1.548 \times$ A2 activity.

Exact calculation of the PARSE score requires the solution of a number of NNLS problems, which presents a potential barrier to use. An approximation to PARSE can be derived by relaxing the non-negative constraint; this approximation requires only a linear combination of gene expression estimates, and is detailed in app:sigs-parse-approx on page 43.

**Validation of the PARSE score** External validation confirmed that the PARSE score was prognostic in other cohorts, including in cancers other than PDAC. PARSE score was significantly prognostic in PDAC cohorts GSE28735 [26] (LRT $P = 0.0149$) and The Cancer Genome Atlas (TCGA) paad (LRT $P = 0.0156$), but not in GSE21501 [22] (LRT $P = 0.115$). When assessed against all TCGA cancers for which at least 50 patients had both an event and complete RNASeq data, the PARSE score was also significantly prognostic for head and neck squamous cell carcinoma, kidney renal clear cell carcinoma, lower grade glioma, and lung adenocarcinoma, at a 5% familywise error rate (FWER) (Table 1.2, column a). This significant result reflected the ability of PARSE score to stratify patients into risk groups in a range of solid tumours, as illustrated in Figure 1.9.

Meta-PCNA is a 130-gene signature of cell proliferation that has been found to be generally prognostic in a number of cancer cohorts [25]. To exclude the possibility that PARSE score simply recapitulated the known meta-PCNA signature, I examined whether PARSE contributed additional prognostic information to meta-PCNA in the large TCGA cohorts. In TCGA kidney renal clear cell carcinoma, lower grade glioma, and lung adenocarcinoma, there was significant evidence that the PARSE score provided prognostic information beyond that given by meta-PCNA, at a 5% FWER (Table 1.2, column b).

Table 1.1: Characteristics of the full APGI patient cohort, and the homogenous PDAC-only subset used for signature discovery. Ordinal variables are shown as median, with quartiles in parentheses. Categorical variables for which percentages do not add up to 100% indicate the presence of minor unlisted categories. Abbreviations: AAC - ampullary adenocarcinoma; IPMN - intraductal papillary mucinous neoplasm; PNET - pancreatic neuroendocrine tumour; PR - Puerto Rico

| Characteristic | | Full APGI | Discovery |
|---|---|---|---|
| Number of patients | | 228 | 110 |
| Gender | Male | 54.8% | 54.6% |
| Ethnicity | Caucasian | 92.3% | 95.4% |
| | Asian | 6.4% | 4.6% |
| | African | 0.9% | 0% |
| Treatment country | Australia | 86.0% | 100% |
| | USA / PR | 12.7% | 0% |
| Age at diagnosis | (years) | 68 (60 - 75) | 67 (61 - 73) |
| Procedure | Whipple | 63.2% | 71.8% |
| Excision margin status | R0 | 76.8% | 62.7% |
| | R1 | 20.6% | 22.7% |
| | R2 | 2.6% | 14.6% |
| Histological type | PDAC | 61.8% | 100% |
| | AAC | 11.0% | 0% |
| | IPMN | 5.7% | 0% |
| | PNET | 5.7% | 0% |
| Histological grade | 1 | 12.0% | 7.3% |
| | 2 | 55.8% | 64.6% |
| | 3 | 30.1% | 27.3% |
| | 4 | 2.1% | 0.8% |
| Location | Head | 64.0% | 84.6% |
| | Ampulla | 11.4% | 0% |
| | Tail | 11.0% | 8.2% |
| | Body | 5.7% | 6.4% |
| Length | (mm) | 33.0 (24.5 - 45.0) | 35.0 (28.0 - 45.0) |
| Invasion | Perineural | 70.3% | 88.1% |
| | Vascular | 62.4% | 67.9% |
| Node involvement | | 69.3% | 77.1% |
| Disease-specific death | | 52.6% | 63.6% |
| Length of follow-up | (days) | 614 (366 - 888) | 632 (402 - 912) |

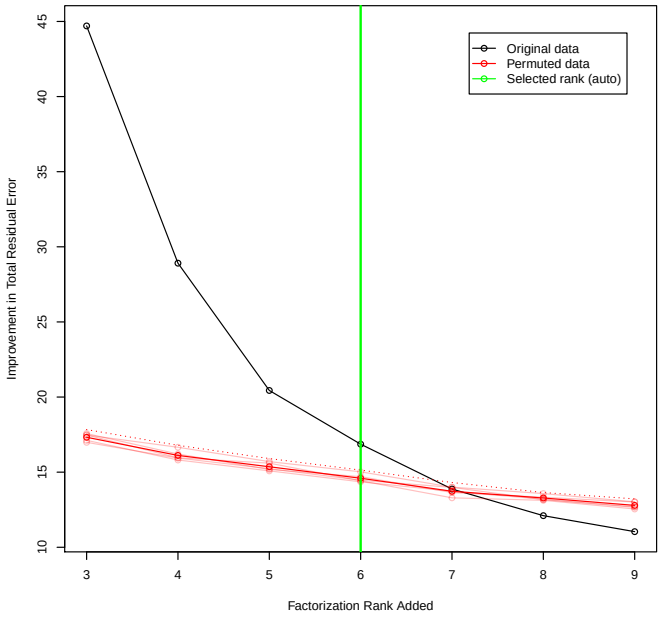


Figure 1.3: Automatic selection of factorization rank. SNMF/L was performed for varying ranks on either unpermuted data (black line) or data permuted within samples (red lines), and the improvement in total residual approximation error $\|A - WH\|_F$ calculated. The highest added rank for which the error improvement on unpermuted data exceeded that of permuted data plus two standard deviations (threshold shown by dotted red line) was the final selected rank (green line).

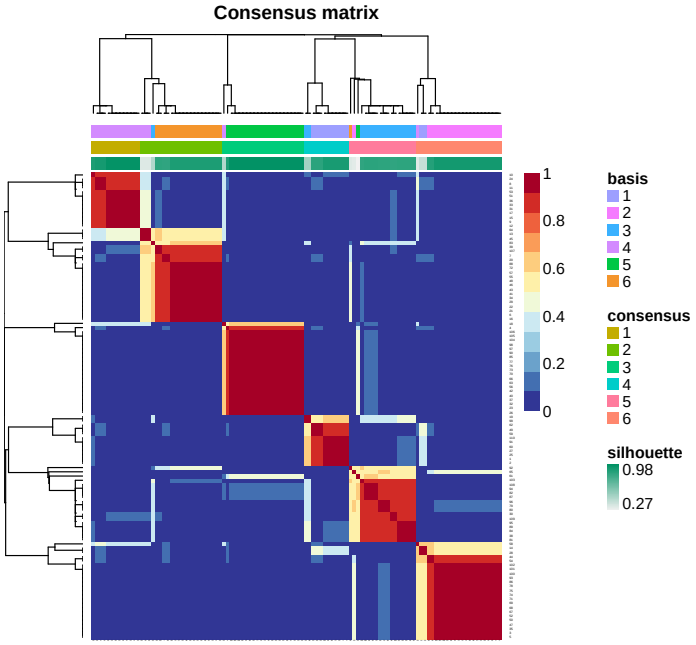


Figure 1.4: Clustering consensus matrix for the final rank-6 clustering. Colours indicate the stability of gene (in rows) and sample (in columns) clusters across random restarts of the factorization; at rank 6 this factorization was largely stable, with identical clusters assigned in all 500 random restarts to the majority of genes and samples.

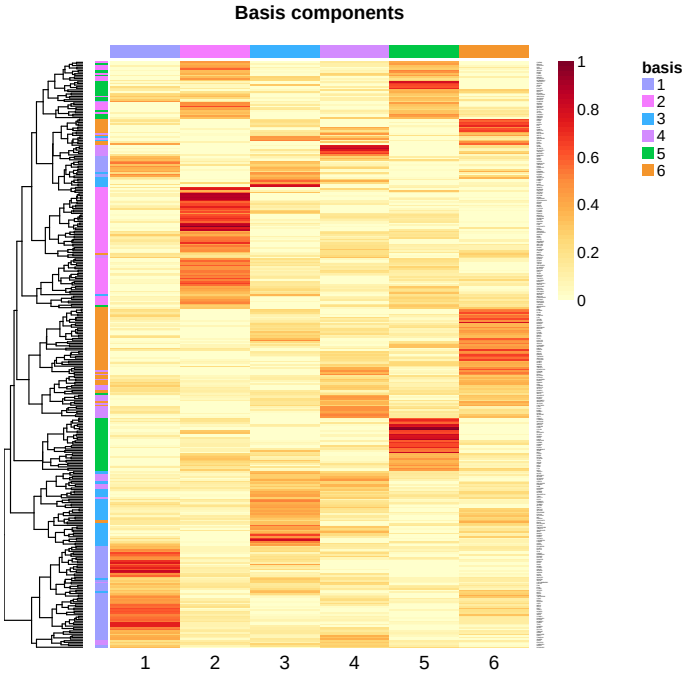


Figure 1.5: Basis matrix $W$ of the final SNMF/L factorization. Rows represent genes, and columns metagenes, with cell colours proportional to the loading of a given gene on a given metagene. The loadings are sparse within rows, indicating that the metagenes are modular, each affecting the expression of largely distinct sets of target genes. A table of values of this basis matrix is available as app:sigs-w-matrix on page 31.

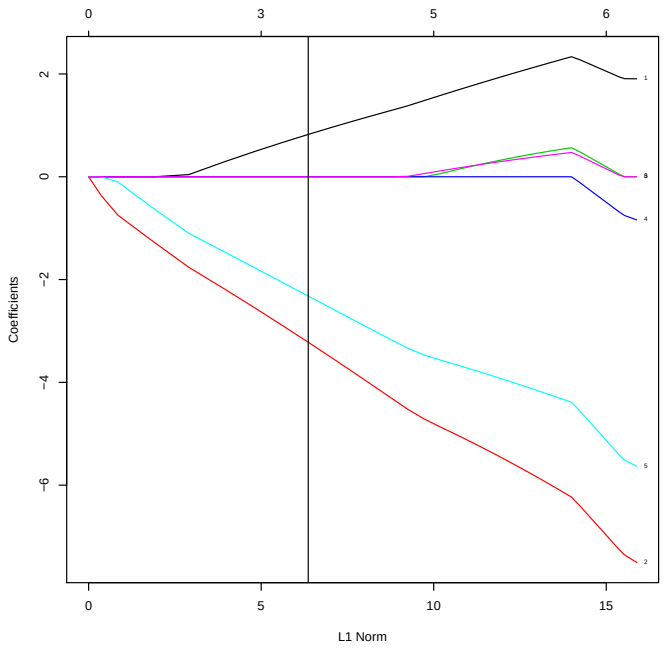


Figure 1.6: Coefficient vs penalty fit trajectories for the LASSO model predicting DSS from metagene expression. Each line represents the model coefficient for a metagene as the model is smoothly varied from a null model (L1 norm = 0), to a full unpenalised Cox fit (L1 norm $\approx$ 16). The vertical line indicates the optimal value of L1 norm as selected by the 1SE criterion on 10-fold cross-validation; at this point in the trajectory only metagenes MG1, MG2, and MG5 contribute to prognosis estimates.

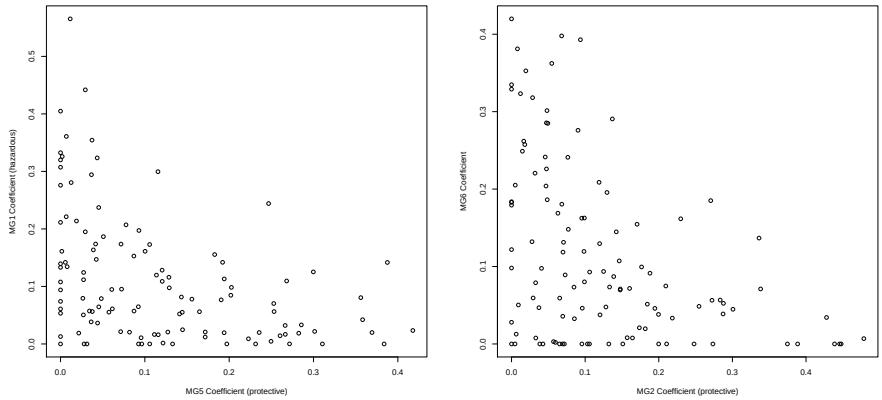


Figure 1.7: Prognostic metagenes form two axes of cell state. Metagene pairs MG1 and MG5, and MG2 and MG6, displayed mutually exclusive coefficient patterns in the APGI cohort, and could be combined to form just two axes of cell state.

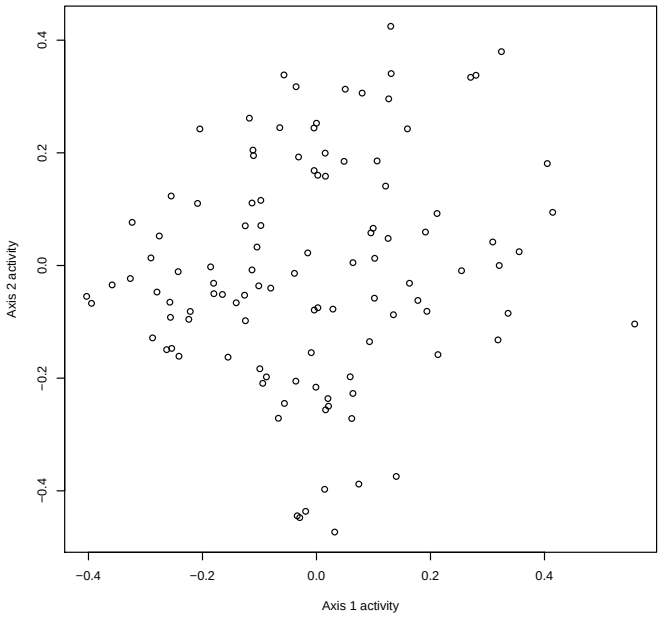


Figure 1.8: Prognostic axis signals are uncorrelated. Activity estimates of axes defined by highly correlated mutually exclusive metagene pairs (Axis A1 = MG1 - MG5, axis A2 = MG6 - MG2) were uncorrelated (Kendall $\tau$ test $P = 0.21$), indicating that these axis signals encoded orthogonal outcome-associated processes within tumours.

Table 1.2: The PARSE score is prognostic in a range of TCGA cancers. P-values are from likelihood ratio tests either comparing a Cox model with PARSE score as a linear predictor, to a null model (a); or a Cox model with PARSE and meta-PCNA scores as linear predictors, against one with meta-PCNA alone (b). Shaded cells are significant at a 5% FWER following Holm's correction. TCGA study codes: *glm*: glioblastoma multiforme; *hnsc*: head and neck squamous cell carcinoma; *kirc*: clear cell kidney carcinoma; *lgg*: lower grade glioma; *luad*: lung adenocarcinoma; *lusc*: lung squamous cell carcinoma; *ov*: ovarian serous cystadenocarcinoma.

| TCGA study | Number of events | Number of patients | Risk score P-value (a) | Improvement P-value (b) |
|---|---|---|---|---|
| gbm | 54 | 143 | 0.2287 | 0.1587 |
| hnsc | 124 | 367 | 8.08E-3 | 0.0108 |
| kirc | 153 | 497 | 2.03E-12 | 2.89E-3 |
| lgg | 53 | 272 | 1.49E-5 | 7.85E-3 |
| luad | 106 | 431 | 8.34E-6 | 1.04E-4 |
| lusc | 117 | 395 | 0.9624 | 0.4110 |
| ov | 115 | 251 | 0.0238 | 0.0178 |

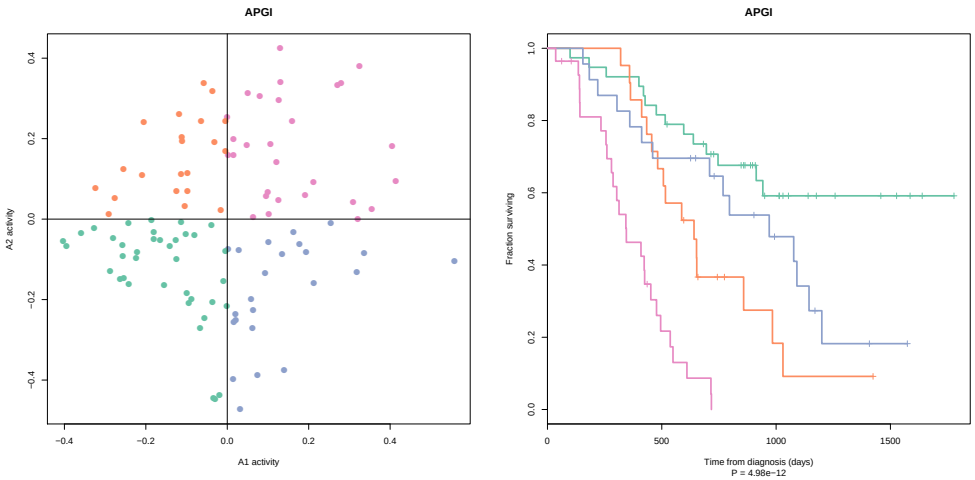


(a) APGI cohort

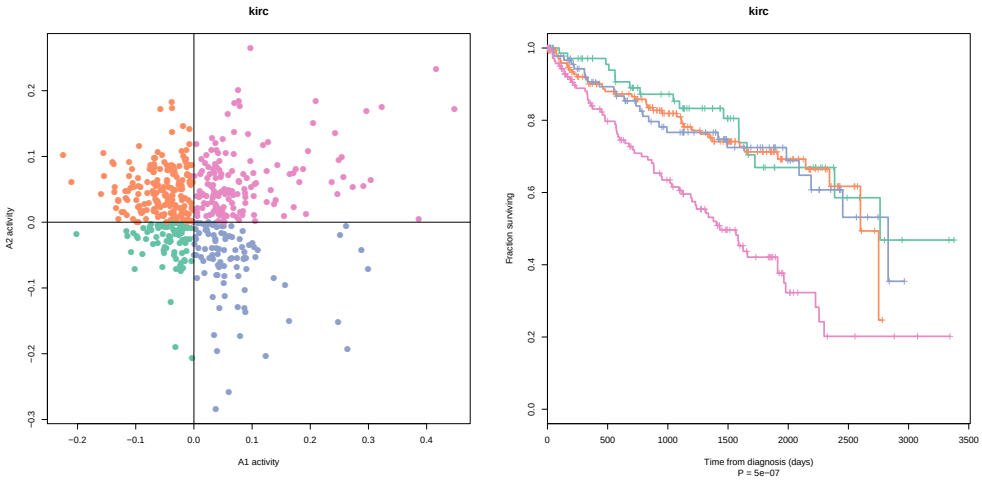


(b) TCGA kirc cohort

Figure 1.9: PARSE score axes define patient subgroups with differing outcome in a range of solid tumours. Activities for axes A1 and A2 of the PARSE score were calculated on the labelled cohorts, and patients split into four subgroups based on the sign of A1 and A2 activities (left panels). The four subgroups thus defined displayed significantly differing clinical courses (right panels). (continued...)

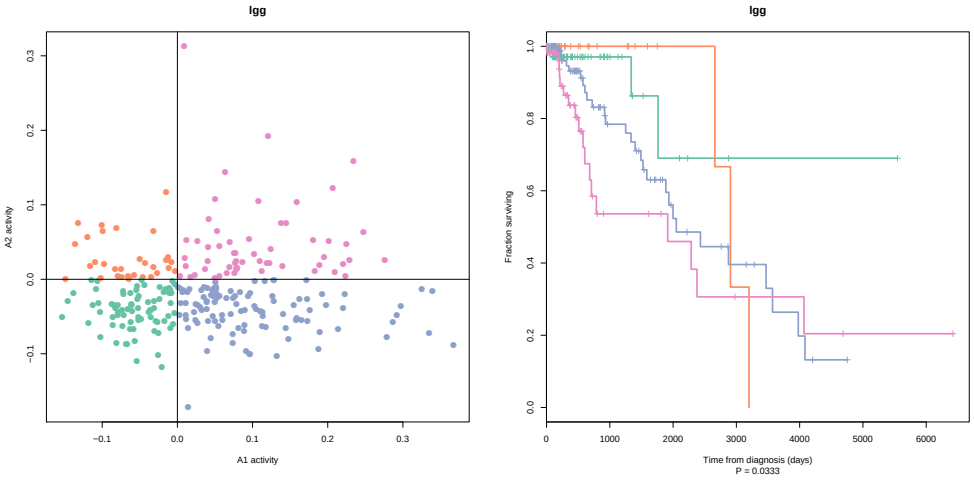


(c) TCGA lgg cohort

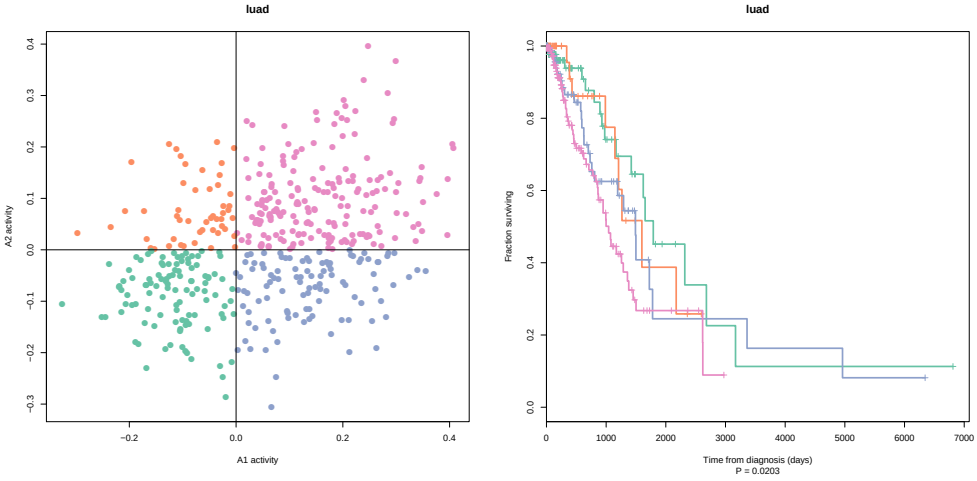


(d) TCGA luad cohort

Figure 1.9: (Concluded). PARSE score axes define patient subgroups with differing outcome in a range of solid tumours. Activities for axes A1 and A2 of the PARSE score were calculated on the labelled cohorts, and patients split into four subgroups based on the sign of A1 and A2 activities (left panels). The four subgroups thus defined displayed significantly differing clinical courses (right panels).

## PARSE identifies proliferation and EMT as fundamental processes controlling survival in PDAC

To link the two prognostic axes that form the PARSE score with potential underlying biology, axis activities on the APGI discovery cohort were compared

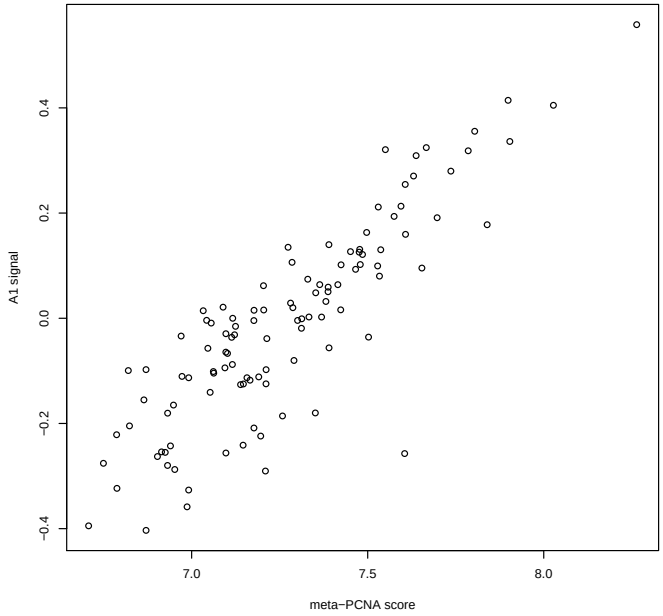


Figure 1.10: Axis A1 signal is closely associated with the meta-PCNA signature. A1 signal and meta-PCNA [25] scores were as evaluated on the APGI training set; Kendall's $\tau = 0.663$, $n = 110$, linear model $R^2 = 0.740$.

to clinical variates, known survival signatures, and scores for signatures from the molecular signatures database (MSigDB) [23].

MSigDB correlations, as well as comparisons to a general proliferative signature, revealed that the PARSE axis A1 (MG1 − MG5) primarily reflected the proliferative state of cells. A1 signal was very strongly correlated with meta-PCNA [25] score (Kendall's $\tau = 0.663$, $n = 110$, Figure 1.10), a relationship supported by its close association to cell cycle-related MSigDB signatures (app:sigs-msigdb-corrs-axis1 on page 40). A1 signal was also significantly positively correlated with qPure [21] estimates of cancer cell fraction in the tumour (Kendall's $\tau = 0.284$, $n = 110$, Table 1.3), although the strength of this association was marginal (linear model $R^2 = 0.155$).

Among the clinical variables tested, PARSE axis A2 (MG6 − MG2) correlated with stromal content and tumour grade: conditions of high A2 signal were associated with higher stromal content, higher grade, and shorter survival. A2 signal was positively correlated with tumour microscopic pathological grade (Holm-corrected $P = 0.0067$, 50 tests performed), although this dependence was weak: on average, A2 signal was 0.1103 higher in grade 3 or 4 tumours over grade 1 or 2, with $R^2 = 0.119$. A2 signal was also negatively associated with tumour cancer cell fraction, the opposite of the positive re-

Table 1.3: Association P-values between metagenes and CPVs. P-values were either from Kendall $\tau$ tests, in the case of continuous or large ordinate clinical variates, or from ANOVA, in the case of categorical variates. Only three associations were signficant at a 5% FWER level by Holm's correction; these are highlighted.

| Variable | Axis 1 | Axis 2 |
|---|---|---|
| Age at diagnosis | 0.925 | 0.666 |
| Ethnicity | 0.771 | 0.113 |
| Gender | 0.158 | 0.010 |
| Histological subtype | 0.697 | 0.157 |
| Invasion | | |
| Perineural | 0.095 | 0.225 |
| Vascular | 0.650 | 0.071 |
| Pack years smoked | 0.356 | 0.275 |
| Pathological grade | $2.39\times10^{-3}$ | $1.30\times10^{-4}$ |
| Cancer cell fraction | $2.13\times10^{-4}$ | $4.11\times10^{-4}$ |
| Recurrence site | | |
| Bone | 0.789 | 0.413 |
| Brain | 0.430 | 0.062 |
| Liver | 0.160 | 0.105 |
| Lung | 0.390 | 0.713 |
| Lymph nodes | 0.933 | 0.870 |
| Mesentery | 0.933 | 0.121 |
| Omentum | 0.139 | 0.082 |
| Other | 0.193 | 0.161 |
| Pancreatic bed | 0.887 | 0.530 |
| Pancreas remnant | 0.534 | 0.184 |
| Peritoneum | 0.916 | 0.015 |
| Staging: M | 0.441 | 0.425 |
| Staging: N | 0.252 | 0.263 |
| Staging: T | 0.264 | 0.427 |
| Staging: Overall stage | 0.061 | 0.236 |
| Tumour location | 0.177 | 0.139 |
| Tumour longest axis length | 0.844 | 0.171 |

lationship observed for axis A1, despite signal in both axes being positively associated with poor prognosis. This reveals a potential context dependency in the influence of stromal content on survival, where high stromal content of a tumour may indicate either good or poor prognosis, depending on which underlying axis is responsible.

A number of MSigDB signatures were associated with A2 signals, among them integrins, extracellular matrix (ECM) processes, and a signature for

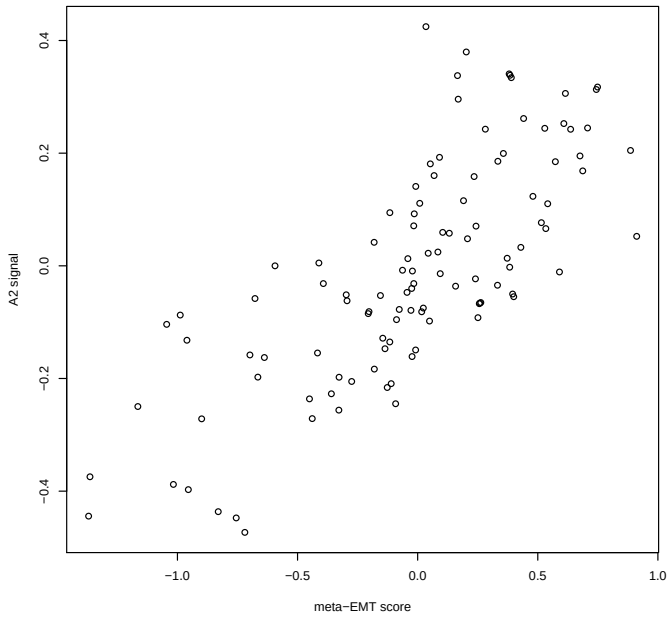


Figure 1.11: Axis A2 signal is closely associated with a signature of the EMT. A2 signal and meta-EMT [7] scores were as evaluated on the APGI training set; Kendall's $\tau = 0.568$, $n = 110$, linear model $R^2 = 0.557$.

LEF1-mediated epithelial to mesenchymal transition (EMT) (app:sigs-msigdb-corrs-axis2 on page 42). Prompted by the strong positive correlation between A2 and the LEF1 overexpression signature, I investigated the association between A2 signal and score for a general signature of EMT, meta-EMT [7]. meta-EMT and A2 signals were strongly positively correlated (Kendall's $\tau = 0.568$, $n = 110$, linear model $R^2 = 0.557$, 1.11), even when cancer cell fraction was taken into account (LRT $P = 9.4 \times 10^{-14}$), strongly indicating that A2 signal predominantly encodes EMT activity. A potential link between A2 and inflammation may also be present: A2 signal was strongly positively correlated with the gene set variation analysis (GSVA) score for MSigDB GNF2_PTX3 (Kendall's $\tau = 0.593$, app:sigs-msigdb-corrs-axis2 on page 42), a proxy for expression of the acute phase response protein pentraxin 3.
1

[1]MP Fatal: TODO: Consider comparing A1 and A2 vs meta-PCNA and meta-ECM in TCGA – are A1/A2 better than the metas? Model complexity is the same so therefore can just compare partials – woo

## 1.3 Discussion

At the molecular level, the phenomenon of cancer has long been recognised as a composite of many processes [8], however the relative importance of each process to a particular type of cancer has been largely uncertain. In pancreas cancer, a huge number of individual biomarkers are known [10], and some attempts have been made to stratify cancers into empirical molecular subtypes [4], but no studies have provided a comprehensive analysis of which basic hallmarks of cancer are actually important in determining patient outcome. This work fills that gap in knowledge, and is the first to exhaustively identify proliferation and the EMT as the major molecular processes that control survival of patients with pancreas cancer.

- PARSE = meta-PCNA + meta-EMT (+ immune + stroma?).
- Context-dependency of stroma signal
- The folly of clustering
- GSE21501 – why didn't it validate?
- Broader implications of pan-cancer survival signature
- Relevance to future work.

## 1.4 Methods

### Cohort recruitment and ethics

[2]

### Sample collection, preparation, and gene expression microarrays

[3]

### Data preprocessing

**Microarray quality control and normalization** Illumina data (IDAT) files were read into Bioconductor `lumi` structures using the `lumidat` package. Seven arrays were excluded on the basis of poor signal, due to fewer than 30% of probes on these arrays having detection P-values of less than 0.01. The

[2] MP Fatal: TODO: Cohort recruitment and ethics
[3] MP Fatal: TODO: Sample collection, preparation, and gene expression microarrays

remaining 234 microarrays represented a range of tumour types, and were normalized as one batch using the `lumi` package. Normalization proceeded serially as: RMA-like background subtraction (`lumiB` method `"bgAdjust.affy"`), variance stabilizing transform (VST) (`lumiT` method `"vst"`), and quantile normalization (`lumiN` method `"quantile"`).

**Unsupervised probe selection** Probes were excluded if they met any of the following criteria: fewer than 10% of samples with expression P-values of less than 0.01, a probe quality (from the `illuminaHumanv4PROBEQUALITY` field in Bioconductor package `illuminaHumanv4.db`) not equal to 'perfect' or 'good', missing gene annotation, or a standard deviation of normalized expression values across all samples of less than 0.03. The choice of this latter threshold is expected to yield approximately a 5% false probe rejection rate, based on an analysis of the variation between technical replicate samples. In cases where multiple post-filter microarray probes mapped to the same gene, only the probe with the highest standard deviation, as evaluated across all samples that passed quality checks, was retained. The effect of these combined filtering steps was to reduce the number of features under consideration from 47,273 probes to 13,000, one per gene.

**Sample selection** From the full set of 234 tumour samples that passed quality checks, eight were from four samples that had each been arrayed twice, and two were from patients with multiple conflicting CPV data. The two with conflicting CPV data were excluded from further study, and the eight replicated samples were averaged, after multidimensional scaling (MDS) indicated that each replicate pair had very similar expression.

The 228 APGI patients for which GEX and clinical data were available were subset further to yield a homogeneous PDAC cohort, suitable for the discovery of the survival-associated processes specific to PDAC. 141 of 228 patients had pathologically confirmed PDAC; of these, five were judged to have suffered a perioperative death, and were not considered further. 110 of the 136 remaining patients were treated in hospitals in Australia, 23 in the USA, two in Italy, and one in Puerto Rico. To eliminate the potential for country-specific gene expression patterns to interact with possible differential survival between countries, only the Australian subset of the cohort was retained, resulting in 110 patients in the final APGI discovery cohort.

**Summary** The above preprocessing steps yielded matched CPV and resected tumour GEX data for 13,000 genes across 110 patients.

### Outcome-associated gene selection

Genes that were associated with DSS were identified by SIS-FAST [6], with a CPSS wrapper to reduce the false positive rate [20]. FAST statistics for

time from diagnosis to DSD were calculated using R package `ahaz` on standardized log-scale expression values; genes which had an absolute statistic value exceeding 7 were selected by the inner SIS-FAST procedure. The outer CPSS wrapper selected genes which were returned by at least 80% of 100 complementary paired SIS-FAST runs. Gene selection FDR was estimated by permutation: 50 repeats of the full gene selection procedure were performed on data in which patients had been randomly shuffled, and the FDR was estimated as the median number of genes selected in permuted runs, divided by the number of genes selected by the unpermuted procedure.

### Rank estimation and metagene factorization

The gene $\times$ patient expression matrix of outcome-associated genes was decomposed into metagenes by the SNMF/L procedure of [12], as implemented in R package `NMF`. SNMF/L is a variant of NMF, a class of procedures that decomposes a non-negative matrix $A$ into a product of non-negative matrices $W$ and $H$, $A \approx WH$. $W$ and $H$ typically have rank much less than $A$, the effect of NMF then being to effectively reduce a large gene $\times$ sample matrix $A$ into smaller matrices, the gene $\times$ metagene basis matrix $W$, and metagene $\times$ sample coefficient matrix $H$. SNMF/L was chosen from the many NMF variants available for its design that favours solutions with sparse $W$: SNMF/L factorizations tend to associate each gene with a small number of metagenes, a situation that matches our biological expectation that, for most genes, expression of that gene is only associated with a small number of biological processes.

As NMF is a linear factorization, the VST-transformed expression matrix $A$ was approximately linearized by elementwise exponentiation, $a_{i,j} \leftarrow 2^{a_{i,j}}$. To reduce the influence of large variations in baseline expression on the factorization, each row (gene) of $A$ was then independently linearly scaled to lie between zero and one, $a_{i,j} \leftarrow (a_{i,j} - \min(a_{i,*})) \div (\max(a_{i,*}) - \min(a_{i,*}))$, where $a_{i,*}$ denotes row $i$ of $A$.

Factorization rank was estimated following [5]: for test ranks ranging from 2 to 9, 5 SNMF/L decompositions were performed, each on a version of the transformed expression matrix in which rows (genes) had been independently permuted within each column (sample). Approximation error for each decomposition was calculated as $\|A - WH\|_F$, and the reduction in approximation error with increasing rank was compared between factorizations of the original data, and those of the 5 permuted data matrices. The highest rank for which the improvement in error achieved by adding that rank to the factorization on the original data, exceeded the improvement seen by adding that rank on the permuted data, taking into account permutation noise, was selected as the final factorization rank. Specifically, let the improvement in approximation error that results in choosing a rank $i$ decomposition over a rank $i-1$ decomposition, on the unpermuted data, be $\Delta_i = \|A - W_{i-1}H_{i-1}\|_F - \|A - W_iH_i\|_F$.

Equivalently, define $\Delta_i^{*j}$ to be the improvement observed when rank $i$ is added to the factorization of $A^{*j}$, the $j^{\text{th}}$ permutation of the data matrix: $\Delta_i^{*j} = \|A^{*j} - W_{i-1}^{*j} H_{i-1}^{*j}\|_F - \|A^{*j} - W_i^{*j} H_i^{*j}\|_F$. Denote the mean and standard deviation of $\Delta_i^*$ across all 5 permutations of the data matrix, for each $i$, as $\overline{\Delta_i^*}$ and $\text{SD}(\Delta_i^*)$, respectively. Then, the final selected rank $k$ was selected as $k = \max(\{i : \Delta_i > \overline{\Delta_i^*} + 2\text{SD}(\Delta_i^*)\})$.

Following rank estimation, a final factorization of the data was performed using only the identified rank, and a larger number of random algorithm restarts, as described below. Subsequent work used this final factorization.

The SNMF/L algorithm requires parameters $\alpha$ and $\eta$ to control regularization; for all factorizations $\alpha = 0.01$, and $\eta = \max(A)$.[4] The default convergence criteria of the `NMF` package were used.

SNMF/L may not necessarily find a global optimum factorization; to address this, multiple random initializations of matrix $W$ were made from $\text{Uniform}(0, \max(A))$, the SNMF/L procedure was run to convergence, and the result with lowest approximation error was retained. 50 random restarts were used during rank estimation runs, and 500 for the final factorization; examination of approximation error distributions for these repeated runs indicated that these values were conservative, and factorizations were robust to the choice of random start.

### Estimating metagene coefficients on new cohort data

To apply the signatures developed in this work to GEX data other than those from the APGI training set, the following procedure was used. GEX measurements from the new cohort were subset to the 361 outcome-associated genes identified by CPSS-SIS-FAST (these genes are listed in app:sigs-w-matrix on page 31), and transformed to a linear scale if necessary. Linear measurements were then scaled within genes to between zero and one, as was performed for metagene factorization. Genes for which no expression data were available (the genes being either filtered out in preprocessing or not measured at all) were assigned scaled expression values of zero. These manipulations yielded a gene $\times$ sample matrix $A'$ with rows matching the gene $\times$ metagene basis matrix $W$ from SNMF/L. The metagene $\times$ sample coefficient matrix $H'$ for the new cohort was then estimated by NNLS implemented in R package `nnls`, solving for each column of $a'_{*,i}$ of $A'$ the optimization problem $h'_{*,i} = \text{argmin}_x \|Wx - a'_{*,i}\|_2$, where $h'_{*,i}$ denotes column $i$ of $H'$. Values of the $W$ matrix used are available as app:sigs-w-matrix on page 31.

For consistency, the above procedure was used to estimate metagene coefficients $H$ for the discovery APGI cohort, as well as all validation cohorts.

[4] Note that this parameter $\alpha$ is denoted $\beta$ in the R `NMF` package; I use the symbol $\alpha$ here for consistency with [12]

### Calculation of the PARSE score on new cohort data

Given metagene coefficients estimated as above, axis activity scores were calculated as Axis A1 activity = MG1 coefficient−MG5 coefficient; Axis A2 activity = MG6 coefficient − MG2 coefficient. PARSE scores were then made by combining axis activity estimates, as PARSE score = $1.354 \times$ A1 activity + $1.548 \times$ A2 activity.

Although not used in this work, a simplified procedure for the approximate calculation of PARSE scores was also developed; see app:sigs-parse-approx on page 43 for details.

### External validation of outcome-associated metagenes

Gene expression data for accessions GSE21501 and GSE28735 were downloaded as processed series matrix data from the National Center for Biotechnology Information (NCBI) Gene Expression Omnibus (GEO). Survival times, censoring indicators, clinical covariates (for GSE21501), and probe expression estimates were extracted from the series matrix files. Probes were annotated with gene symbols using the associated GPL annotation files, and probes with no gene annotation were discarded. If multiple probes mapped to the same gene symbol, only the probe with the highest standard deviation across all samples in a data set was retained. Finally, only probes with a standard deviation within the top $20^{\text{th}}$ percentile within a data set were kept for metagene scoring.

Gene expression and outcome data for all TCGA cancers were downloaded from the public TCGA open-access repository at `https://tcga-data.nci.nih.gov/tcgafiles/ftp_auth/distro_ftpusers/anonymous/tumor/`, on 18 November 2014. RNASeq Version 2 Level 3 expression estimates (on an approximately linear scale) from Illumina HiSeq machines only were used, without further processing. Expression estimates were scaled within genes to between 0 and 1 separately within each TCGA cancer type. For reasons of statistical power, only TCGA cancers for which at least 50 patients had both complete RNASeq expression data, and an event, were considered in validation. Cohort paad was included despite it not meeting this criterion, to allow validation against another PDAC cohort.

For each validation data set, metagene coefficients, axis activities, and PARSE scores, were calculated as described above. Prognostic performance of the PARSE score was tested within each validation data set using likelihood ratio tests comparing a Cox model using PARSE score as the sole linear covariate, with an intercept-only Cox model.

### GSVA scoring

The expression of gene sets from the MSigDB [23] were estimated on the APGI cohort using a modification of the GSVA method [9]. GSVA with default set-

tings was used to estimate expression scores for all MSigDB gene sets in the full 13,000 × 228 VST-scaled APGI GEX data matrix. MSigDB contains both undirected gene sets such as metabolic pathways, in which members of the set are not expected a-priori to move in concert, and directional signatures, with paired `*_UP` and `*_DN` components that would be expected to change in coordinated and opposite patterns. Conventional analyses based on MSigDB ignore this distinction, but for this work I combined paired directional signatures to yield an overall signed estimate of signature activity. For undirected signatures, GSVA activity estimates were simply calculated using parameter `abs.ranking=TRUE`. In the case of paired signatures, GSVA scores were estimated separately for the `*_UP` and `*_DN` sets using parameter `abs.ranking=FALSE`, and the signed combined activity `*_SIGNED` was calculated as the `*_DN` score subtracted from the `*_UP` score. This procedure resulted in summarised activity estimates for 8,138 gene sets, many of which were highly correlated.

Gene sets with highly correlated activity scores were collapsed into compound summary sets as follows. Pairwise Pearson correlation distances between all scores were calculated as $d_{i,j} = \frac{1}{2}(1 - \text{cor}(s_i, s_j))$, and were used to cluster gene sets using R `hclust` and complete linkage. R `cutree` identified clusters of highly similar gene sets, using a distance threshold of 0.02; gene set activities within each cluster were merged by taking median values across all samples, to form a new merged gene set activity estimate. Following merging, 7,633 single and compound gene set activity estimates remained across 228 samples.

## meta-PCNA and meta-ECM score calculation

Scores for the meta-PCNA signature were calculated from GEX data as described in [25]. To estimate meta-ECM scores, log-scale GEX data were median centered, and then median values across samples were calculated for all genes in the two lists of [7] Table S3, to yield EMT-overexpressed, and EMT-underexpressed, gene list median expression estimates per sample. The meta-ECM score was then calculated as the EMT-overexpressed median value, less the EMT-underexpressed median value.

## Prognostic axis functional characterization

**Clinical variate comparisons** Prognostic axis activities calculated on the APGI data were tested for association with a restricted set of the available APGI CPVs, as outlined in Table 1.4. Numeric variables were tested for assocation with each axis by Kendall's $\tau$ test; factor and boolean variables using ANOVA with the CPV as the explanatory variable. 50 tests in total were performed (25 variables, 2 axes), and P-values were corrected together

using the Holm-Bonferroni procedure [11]. Corrected P-values of less than 0.05 were considered significant.

Table 1.4: CPVs tested for association with prognostic axis signals.

| Clinical variate | Type |
|---|---|
| Age at diagnosis | Ordinal |
| Ethnicity | Factor |
| Gender | Boolean |
| Histological subtype | Factor |
| Invasion: | |
| Perineural | Boolean |
| Vascular | Boolean |
| Pack years smoked | Ordinal |
| Pathological grade | Boolean |
| Recurrence found in: | |
| Bone | Boolean |
| Brain | Boolean |
| Liver | Boolean |
| Lung | Boolean |
| Lymph nodes | Boolean |
| Mesentery | Boolean |
| Omentum | Boolean |
| Other | Boolean |
| Pancreas remnant | Boolean |
| Pancreatic bed | Boolean |
| Peritoneum | Boolean |
| Staging: M | Boolean |
| Staging: N | Boolean |
| Staging: T | Factor |
| Staging: Overall stage | Factor |
| Tumour location | Boolean |
| Tumour longest axis length | Ordinal |

**MSigDB signature score comparisons** Kendall correlation coefficients were calculated between axis activity estimates and GSVA scores for MSigDB gene sets, on the APGI expression dataset. A subset of the full MSigDB was used, as outlined in Table 1.5. Absolute correlations of greater than 0.5 were deemed substantive and reported for further characterisation.

Table 1.5: The subset of MSigDB signatures tested for association with axis activities. Within each MSigDB class, only those matching the indicated inclusion pattern were tested. * represents a wildcard; — matches nothing.

| MSigDB class | Signature name inclusion pattern |
|---|---|
| c1 | — |
| c2 | KEGG_*, PID_*, REACTOME_* |
| c3 | * |
| c4 | GNF2_*, MORF_* |
| c5 | * |
| c6 | * |
| c7 | * |

### Attribution of work

Data for the APGI discovery cohort were generated as part of the APGI project, under the umbrella of the International Cancer Genome Consortium (ICGC). The generation of these data was a huge team effort, of which I only played a small part. However, all steps subsequent to raw data generation, from low level processing of IDAT files through to analysis planning, signature development, testing, and interpretation, were performed solely by me.

# Appendices

# Appendix A

# Basis matrix $W$ for the six survival-associated metagenes

| | MG1 | MG2 | MG3 | MG4 | MG5 | MG6 |
|---|---|---|---|---|---|---|
| A4GALT | 0.0295 | 0.0000 | 1.2977 | 0.0788 | 0.3625 | 0.5232 |
| A4GNT | 0.0000 | 0.7419 | 0.0483 | 0.0539 | 0.3720 | 0.0666 |
| ABHD16A | 0.6623 | 0.7249 | 0.0000 | 0.0000 | 0.5217 | 0.2210 |
| ABHD5 | 0.1481 | 0.7473 | 0.0000 | 0.7478 | 0.3988 | 1.1727 |
| ABLIM1 | 0.0145 | 0.9135 | 0.3159 | 0.0000 | 0.6066 | 0.3419 |
| ACE | 0.0333 | 0.8332 | 0.0536 | 0.0000 | 0.0000 | 0.1814 |
| ACKR3 | 0.0029 | 0.0000 | 0.3821 | 0.3591 | 0.2080 | 0.5772 |
| ACYP2 | 0.2481 | 0.8949 | 0.0000 | 0.2334 | 0.8454 | 0.4110 |
| ADH1A | 0.0730 | 0.4440 | 0.0052 | 0.1009 | 0.6614 | 0.0000 |
| ADM | 0.0000 | 0.0000 | 0.5168 | 0.5137 | 0.0000 | 0.3570 |
| AGRP | 0.0000 | 0.0000 | 0.0000 | 0.6786 | 0.0000 | 0.1744 |
| AKIP1 | 0.6365 | 0.2394 | 0.6036 | 0.7118 | 0.7849 | 0.7168 |
| AKR1A1 | 0.2470 | 1.0849 | 0.2633 | 0.2921 | 0.6588 | 0.4524 |
| ALDH5A1 | 0.0988 | 0.9930 | 0.5463 | 0.0566 | 0.8968 | 0.2222 |
| ALOX5AP | 0.0525 | 0.0084 | 0.0147 | 1.2654 | 0.3441 | 0.7138 |
| AMOT | 0.0653 | 0.8246 | 0.1374 | 0.5176 | 0.4311 | 0.5705 |
| ANGPTL2 | 0.0000 | 0.0000 | 0.3694 | 0.8726 | 0.1807 | 0.9222 |
| ANGPTL4 | 0.1789 | 0.0000 | 0.4156 | 0.0461 | 0.0260 | 0.3906 |
| ANKLE2 | 0.7503 | 0.1422 | 0.6238 | 0.5082 | 0.1879 | 0.3839 |
| ANKRD22 | 0.4067 | 1.3536 | 0.1731 | 0.2672 | 0.0381 | 0.2229 |
| ANKRD37 | 0.0562 | 0.1817 | 0.2150 | 0.7249 | 0.0129 | 0.5715 |
| ANLN | 1.1696 | 0.2368 | 0.0796 | 0.0772 | 0.0000 | 0.7203 |
| APCDD1 | 0.0000 | 0.1375 | 0.1494 | 0.1308 | 0.5957 | 0.8366 |
| APCS | 0.0000 | 0.0306 | 0.1569 | 0.1001 | 0.1638 | 0.3521 |
| ARFGAP3 | 0.0252 | 0.2988 | 0.5370 | 0.8377 | 0.4872 | 0.5353 |
| ARHGAP24 | 0.0628 | 1.0614 | 0.0157 | 0.7487 | 1.1007 | 0.6209 |

| | | | | | | |
|---|---|---|---|---|---|---|
| ARHGEF19 | 0.0837 | 0.0833 | 1.2033 | 0.5242 | 0.4520 | 0.5071 |
| ARL4C | 0.0000 | 0.0171 | 0.3025 | 0.4910 | 0.2953 | 1.2264 |
| ARSD | 0.1550 | 1.2389 | 0.1919 | 0.0000 | 0.2154 | 0.1439 |
| ASPM | 1.1736 | 0.3897 | 0.2026 | 0.1743 | 0.0380 | 0.0396 |
| ATAD2 | 0.9358 | 0.0696 | 0.1136 | 0.0265 | 0.1092 | 0.3070 |
| ATF7IP2 | 0.0000 | 0.2019 | 0.1165 | 0.0000 | 0.0319 | 0.0000 |
| ATL3 | 0.6429 | 0.0252 | 0.1566 | 0.4867 | 0.2467 | 0.2863 |
| AURKB | 1.0027 | 0.1107 | 0.1351 | 0.0000 | 0.0096 | 0.0000 |
| AXIN2 | 0.0000 | 0.5221 | 0.4413 | 0.1313 | 0.8077 | 0.2911 |
| B3GALTL | 0.3601 | 0.3276 | 0.5636 | 0.3806 | 0.4898 | 0.7750 |
| BAMBI | 0.1091 | 0.0034 | 0.8430 | 0.3931 | 0.2428 | 0.1686 |
| BBS2 | 0.2474 | 1.1417 | 0.0000 | 0.2202 | 1.0006 | 1.1598 |
| BCKDK | 0.2186 | 0.2923 | 0.8654 | 1.0655 | 0.4050 | 0.1090 |
| BCL11B | 0.1982 | 0.9231 | 0.2260 | 0.2401 | 0.4151 | 0.0000 |
| BIRC5 | 1.3802 | 0.1694 | 0.3679 | 0.5452 | 0.0000 | 0.2427 |
| BOC | 0.0000 | 0.0000 | 0.3211 | 0.0000 | 1.6086 | 0.0000 |
| BTN3A1 | 0.6641 | 0.7077 | 0.0729 | 0.2544 | 0.9928 | 0.2964 |
| C1orf56 | 0.0000 | 0.8742 | 0.0000 | 0.3677 | 0.1145 | 0.3590 |
| C1QTNF6 | 0.0000 | 0.0000 | 0.5885 | 0.6205 | 0.2234 | 0.9726 |
| C2orf70 | 0.1081 | 1.0889 | 0.0206 | 0.0000 | 0.0000 | 0.0000 |
| C5orf46 | 0.0000 | 0.0000 | 0.0000 | 1.0562 | 0.1278 | 1.0438 |
| C9orf152 | 0.2087 | 1.3686 | 0.0000 | 0.3548 | 0.0206 | 0.0000 |
| CA8 | 0.0000 | 0.6859 | 0.0502 | 0.0094 | 0.0536 | 0.0000 |
| CACHD1 | 0.0000 | 0.6891 | 0.0153 | 0.0000 | 1.0768 | 0.4880 |
| CADPS2 | 0.2591 | 1.2923 | 0.0000 | 0.5506 | 1.0209 | 0.5729 |
| CAMK1G | 0.0940 | 0.2377 | 0.0000 | 0.0316 | 0.8847 | 0.0000 |
| CAPN6 | 0.0000 | 0.7541 | 0.0000 | 0.2282 | 0.6418 | 0.0000 |
| CARHSP1 | 0.7535 | 0.5316 | 0.8652 | 0.8993 | 0.2633 | 0.0000 |
| CATSPER1 | 0.1179 | 0.0000 | 0.9199 | 0.0000 | 0.0000 | 0.1046 |
| CAV1 | 0.4195 | 0.0000 | 0.1925 | 0.0801 | 0.2714 | 0.8420 |
| CCDC88A | 0.0000 | 0.1729 | 0.4668 | 0.0109 | 0.8006 | 1.0201 |
| CCL19 | 0.0000 | 0.0000 | 0.0000 | 0.0000 | 0.9529 | 0.0000 |
| CCNB1 | 1.4334 | 0.4638 | 0.1274 | 0.2506 | 0.0155 | 0.3645 |
| CCR7 | 0.0569 | 0.0000 | 0.0000 | 0.0000 | 1.0524 | 0.0000 |
| CD70 | 0.0870 | 0.0000 | 0.2096 | 0.3612 | 0.0000 | 0.4343 |
| CDA | 0.2927 | 0.0000 | 0.3408 | 0.0000 | 0.0000 | 0.6991 |
| CDC45 | 0.9608 | 0.0779 | 0.1086 | 0.3364 | 0.0336 | 0.0000 |
| CDK12 | 0.1906 | 0.2755 | 0.0000 | 0.0788 | 0.8330 | 0.0000 |
| CDK2 | 1.0635 | 0.2517 | 0.0111 | 0.5230 | 0.3310 | 0.3338 |
| CEBPB | 0.0729 | 0.0654 | 1.2909 | 0.5287 | 0.5065 | 0.8131 |
| CEP55 | 1.4198 | 0.3340 | 0.0000 | 0.1690 | 0.0000 | 0.4555 |
| CFDP1 | 0.3512 | 0.5466 | 0.7440 | 0.6706 | 0.0000 | 0.2594 |
| CHAF1B | 0.9890 | 0.2957 | 0.1997 | 0.0187 | 0.5165 | 0.0960 |
| CHEK1 | 1.5161 | 0.1621 | 0.0000 | 0.0034 | 0.1080 | 0.2731 |

| | | | | | | |
|---|---|---|---|---|---|---|
| CHN2 | 0.0000 | 0.4963 | 0.0000 | 0.3389 | 0.4366 | 0.0000 |
| CIDEC | 0.0279 | 0.0000 | 0.4258 | 0.2777 | 0.0038 | 0.0000 |
| CIDECP | 0.1140 | 0.0232 | 0.5161 | 0.2795 | 0.1093 | 0.0000 |
| CKAP2L | 1.7829 | 0.2230 | 0.2724 | 0.0319 | 0.0000 | 0.0884 |
| CLEC3B | 0.0589 | 0.0691 | 0.1151 | 0.0110 | 0.8063 | 0.0000 |
| CNIH3 | 0.0000 | 0.0591 | 0.0000 | 0.3178 | 0.0000 | 0.6014 |
| CNNM1 | 0.0000 | 0.8666 | 0.4109 | 0.0000 | 0.0897 | 0.0000 |
| COL12A1 | 0.0000 | 0.1328 | 0.0340 | 0.5329 | 0.1874 | 1.6461 |
| COL5A3 | 0.0000 | 0.0000 | 0.1816 | 0.0351 | 0.0660 | 1.0286 |
| COL7A1 | 0.0000 | 0.0000 | 0.5858 | 0.0000 | 0.0000 | 0.5878 |
| COLGALT1 | 0.3987 | 0.1554 | 0.6227 | 0.4286 | 0.1646 | 0.8792 |
| COLGALT2 | 0.0000 | 0.6011 | 0.0000 | 0.0199 | 0.0000 | 0.0000 |
| COX4I2 | 0.0000 | 0.1744 | 0.0740 | 0.0000 | 0.9855 | 0.3346 |
| CSNK1D | 0.2122 | 0.3756 | 1.5627 | 0.4799 | 0.1570 | 0.2284 |
| CST6 | 0.0651 | 0.0000 | 0.2022 | 0.0000 | 0.0690 | 0.6328 |
| CTSL | 0.3897 | 0.0000 | 0.1976 | 1.1757 | 0.4702 | 0.2240 |
| CTSV | 0.3015 | 0.0439 | 0.2623 | 0.0203 | 0.0194 | 0.1819 |
| CYP2S1 | 0.3223 | 1.0232 | 0.1543 | 0.0000 | 0.0927 | 0.0000 |
| DCAF8 | 0.0000 | 1.1369 | 0.4818 | 0.1094 | 0.5277 | 0.1875 |
| DCBLD2 | 0.4024 | 0.0000 | 0.1236 | 0.0000 | 0.1426 | 0.8437 |
| DCUN1D5 | 1.3599 | 0.0751 | 0.0000 | 0.8575 | 0.9561 | 0.7193 |
| DENND1A | 0.8191 | 0.0000 | 0.2458 | 0.1898 | 0.0000 | 0.1782 |
| DERA | 1.1839 | 0.1952 | 0.4571 | 0.6042 | 0.2890 | 0.3195 |
| DHRS9 | 0.0000 | 0.0000 | 0.9957 | 0.3426 | 0.0000 | 0.1699 |
| DKK1 | 0.4779 | 0.0000 | 0.2976 | 0.1847 | 0.0000 | 0.0242 |
| DNAJC9 | 0.7779 | 0.1108 | 0.3734 | 0.1159 | 0.1329 | 0.1528 |
| DPY19L1 | 0.3414 | 0.3625 | 0.2993 | 0.5360 | 0.0781 | 0.5087 |
| DSG2 | 0.4320 | 0.5696 | 0.1794 | 0.5147 | 0.0387 | 0.7066 |
| DSG3 | 0.1766 | 0.0000 | 0.2140 | 0.0000 | 0.0000 | 0.5384 |
| DYNC2H1 | 0.0000 | 1.6131 | 0.1497 | 0.0000 | 0.7591 | 0.6693 |
| E2F7 | 1.0366 | 0.0000 | 0.0315 | 0.0222 | 0.0000 | 0.5360 |
| EDIL3 | 0.0000 | 0.0000 | 0.0000 | 0.8576 | 0.0121 | 0.8163 |
| EIF2AK3 | 0.1806 | 1.2690 | 0.0000 | 0.3842 | 0.6143 | 0.3321 |
| ELMOD3 | 0.0000 | 1.1608 | 0.6902 | 0.3859 | 0.5348 | 0.0874 |
| EMP3 | 0.2499 | 0.0000 | 0.4619 | 0.1582 | 0.2170 | 0.5646 |
| ENO2 | 0.3608 | 0.3375 | 0.7898 | 0.0339 | 0.0000 | 0.9442 |
| EPHX2 | 0.0000 | 0.5912 | 0.1080 | 0.1660 | 0.6761 | 0.0000 |
| ERRFI1 | 0.1599 | 0.0301 | 0.5475 | 0.3478 | 0.2866 | 0.7895 |
| EXOSC8 | 0.9336 | 0.6010 | 0.2789 | 1.0216 | 0.3682 | 0.1481 |
| EYA3 | 0.0000 | 0.0869 | 0.5323 | 0.0000 | 0.0000 | 0.9120 |
| FAH | 0.6763 | 0.4158 | 0.3555 | 0.2131 | 0.3240 | 0.3914 |
| FAM120AOS | 0.1803 | 1.0488 | 0.0000 | 0.2845 | 0.7143 | 0.5698 |
| FAM134B | 0.0000 | 0.8232 | 0.0000 | 0.2342 | 0.2083 | 0.0000 |
| FAM189A2 | 0.0000 | 1.0020 | 0.0000 | 0.0213 | 0.1143 | 0.0000 |

| | | | | | | |
|---|---|---|---|---|---|---|
| FAM83A | 0.2461 | 0.0000 | 0.1165 | 0.0000 | 0.0000 | 0.2211 |
| FAM91A1 | 0.9811 | 0.1968 | 0.1603 | 0.7865 | 0.0000 | 0.2703 |
| FBXO22 | 0.5017 | 0.3643 | 0.0000 | 0.5761 | 0.0000 | 0.3137 |
| FBXW8 | 0.2492 | 0.2604 | 0.6553 | 0.9331 | 0.1844 | 0.3307 |
| FEM1B | 0.3031 | 0.3008 | 0.0000 | 0.0017 | 0.0838 | 1.4170 |
| FER | 0.4975 | 0.1005 | 0.1802 | 0.4440 | 0.1792 | 0.8664 |
| FGB | 0.0000 | 0.0000 | 0.0170 | 0.3212 | 0.0000 | 0.0818 |
| FGD6 | 0.5544 | 0.0000 | 0.1308 | 0.1418 | 0.0000 | 0.4991 |
| FGG | 0.0548 | 0.0379 | 0.0000 | 0.1372 | 0.0068 | 0.2157 |
| FHDC1 | 0.1771 | 1.2361 | 0.2174 | 0.0189 | 0.0000 | 0.0512 |
| FLRT3 | 0.7913 | 0.1342 | 0.5121 | 0.2846 | 0.2220 | 0.3125 |
| FRZB | 0.0889 | 0.2374 | 0.0000 | 0.5404 | 1.4969 | 0.0017 |
| FSCN1 | 0.3709 | 0.0737 | 1.0622 | 0.1342 | 0.1423 | 0.7358 |
| FST | 0.0000 | 0.0000 | 0.1578 | 0.0000 | 0.0414 | 0.4947 |
| FYN | 0.0127 | 0.5194 | 0.1203 | 0.1287 | 1.6862 | 0.8654 |
| GAB2 | 0.0435 | 0.7351 | 0.3850 | 0.6361 | 1.3628 | 0.2664 |
| GABPB1 | 0.7363 | 0.1963 | 0.0000 | 0.7422 | 0.2159 | 0.6724 |
| GAPDH | 0.4758 | 0.3945 | 0.8305 | 0.2369 | 0.0000 | 0.7231 |
| GATA6 | 0.0534 | 0.8827 | 0.0860 | 0.1396 | 0.1932 | 0.0000 |
| GATC | 1.0220 | 0.1104 | 0.0000 | 0.4818 | 0.0723 | 0.4716 |
| GIMAP2 | 0.1486 | 0.7215 | 0.0000 | 0.6567 | 0.7701 | 0.0000 |
| GINS2 | 1.0803 | 0.1777 | 0.3933 | 0.0729 | 0.0000 | 0.0000 |
| GNPAT | 0.1710 | 0.9518 | 0.1369 | 0.4352 | 0.1758 | 0.1925 |
| GOLM1 | 0.0000 | 0.7145 | 0.1203 | 0.0488 | 0.0000 | 0.0000 |
| GPC3 | 0.0980 | 0.2322 | 0.0000 | 0.0000 | 1.2713 | 0.0000 |
| GPR176 | 0.4324 | 0.3072 | 0.0000 | 0.7415 | 0.3745 | 0.5882 |
| HIPK2 | 0.2587 | 1.2502 | 0.0694 | 0.2371 | 0.5213 | 0.0000 |
| HJURP | 1.3269 | 0.2436 | 0.2326 | 0.0210 | 0.0000 | 0.0000 |
| HRASLS2 | 0.3273 | 0.0000 | 0.3045 | 0.2167 | 0.0000 | 0.0000 |
| HSP90B1 | 0.5274 | 0.4642 | 0.7758 | 0.8972 | 0.2977 | 0.3795 |
| HSPB6 | 0.0000 | 0.1493 | 0.1298 | 0.0000 | 1.3081 | 0.3131 |
| ICAM2 | 0.5013 | 0.1959 | 0.4755 | 0.3105 | 0.4043 | 0.1342 |
| IDH2 | 0.7131 | 0.4322 | 0.3970 | 0.2145 | 0.3314 | 0.2342 |
| IFT140 | 0.0000 | 1.0890 | 0.5193 | 0.0000 | 0.2592 | 0.0662 |
| IGFBP1 | 0.2708 | 0.0000 | 0.2323 | 0.0327 | 0.0000 | 0.0058 |
| IGLL3P | 0.1660 | 0.1496 | 0.0000 | 0.0000 | 0.7633 | 0.0000 |
| IKBIP | 0.2893 | 0.0000 | 0.3028 | 1.1219 | 0.1455 | 0.4694 |
| IL1R2 | 0.0377 | 0.2543 | 0.4285 | 0.2301 | 0.0000 | 0.0605 |
| IL20RB | 0.2578 | 0.0000 | 0.3094 | 0.0000 | 0.0000 | 0.6805 |
| IL33 | 0.2369 | 0.0436 | 0.0000 | 0.1304 | 0.6759 | 0.0000 |
| ITGA5 | 0.0000 | 0.0000 | 0.4758 | 0.2666 | 0.1206 | 0.6815 |
| ITPKB | 0.0000 | 0.8315 | 0.6059 | 0.0000 | 1.1923 | 0.6724 |
| KANK4 | 0.0000 | 0.0000 | 0.1981 | 0.4683 | 0.0000 | 1.2292 |
| KCNQ3 | 0.0000 | 0.1296 | 0.1721 | 0.7768 | 0.0916 | 0.5160 |

| | | | | | | |
|---|---|---|---|---|---|---|
| KCTD10 | 0.3776 | 0.1324 | 0.2867 | 0.4387 | 0.5081 | 0.7943 |
| KCTD5 | 0.3848 | 0.5133 | 1.1253 | 0.6056 | 0.0000 | 0.0000 |
| KIAA0513 | 0.0828 | 1.0351 | 0.1715 | 0.3220 | 0.5910 | 0.0000 |
| KIAA1549L | 0.3755 | 0.0812 | 0.2646 | 0.6647 | 0.1501 | 0.6423 |
| KIF14 | 1.1244 | 0.3648 | 0.1952 | 0.4293 | 0.0000 | 0.1264 |
| KIF20A | 1.3726 | 0.2864 | 0.2082 | 0.2320 | 0.0000 | 0.2888 |
| KIF2C | 0.7952 | 0.1329 | 0.1096 | 0.0074 | 0.0000 | 0.0000 |
| KLHL5 | 0.4215 | 0.1645 | 0.0000 | 0.3538 | 0.6955 | 1.1410 |
| KNTC1 | 1.0718 | 0.1383 | 0.4419 | 0.0827 | 0.1499 | 0.2787 |
| KRT17 | 0.2860 | 0.0000 | 0.3863 | 0.1586 | 0.1201 | 0.5074 |
| KRT6A | 0.1386 | 0.0000 | 0.1202 | 0.0000 | 0.0000 | 0.4668 |
| KRT6C | 0.1187 | 0.0000 | 0.0000 | 0.0000 | 0.0000 | 0.1640 |
| KRT7 | 0.4597 | 0.0020 | 0.5620 | 0.0000 | 0.1354 | 0.4370 |
| KYNU | 0.6104 | 0.0894 | 0.0693 | 0.5431 | 0.0000 | 0.2790 |
| LAMA5 | 0.3670 | 0.0772 | 1.0234 | 0.0000 | 0.3418 | 0.1832 |
| LCNL1 | 0.1072 | 0.2829 | 0.0115 | 0.2669 | 0.5289 | 0.0000 |
| LDHA | 0.6526 | 0.4664 | 0.0000 | 0.3186 | 0.0504 | 1.1696 |
| LETM2 | 0.4402 | 0.0000 | 0.3924 | 0.0000 | 0.0000 | 0.2831 |
| LGALS9B | 0.1106 | 1.0239 | 0.0000 | 0.0000 | 0.3463 | 0.4913 |
| LINC01184 | 0.6331 | 0.8045 | 0.0000 | 0.3418 | 0.8076 | 0.0000 |
| LMO3 | 0.0000 | 0.1062 | 0.0000 | 0.0090 | 1.1796 | 0.0136 |
| LMTK2 | 0.7364 | 0.3642 | 0.3100 | 0.5254 | 0.0204 | 0.2425 |
| LOC100506562 | 0.5772 | 0.2935 | 0.6002 | 0.6045 | 0.1075 | 0.1108 |
| LOX | 0.2078 | 0.0000 | 0.0806 | 0.3896 | 0.0866 | 0.9212 |
| LYNX1 | 0.0337 | 0.0000 | 0.2575 | 0.1651 | 0.0000 | 0.0951 |
| MAP3K8 | 0.1984 | 0.0000 | 0.0681 | 0.3075 | 0.5588 | 0.4348 |
| MARCKSL1 | 0.1504 | 1.3374 | 0.2978 | 0.0000 | 0.0000 | 0.2627 |
| MARS2 | 0.7481 | 1.0181 | 0.0000 | 0.4007 | 0.4981 | 0.0000 |
| MC1R | 0.1042 | 0.1313 | 1.0794 | 0.8656 | 0.4740 | 0.1335 |
| MCEMP1 | 0.0000 | 0.0000 | 0.0000 | 0.6056 | 0.0000 | 0.2992 |
| MCM10 | 1.1446 | 0.1414 | 0.0000 | 0.0141 | 0.0000 | 0.0808 |
| MCM4 | 1.2790 | 0.1411 | 0.3090 | 0.0254 | 0.0103 | 0.1276 |
| MCOLN2 | 0.1988 | 0.2778 | 0.0000 | 0.0000 | 0.9442 | 0.0000 |
| MELK | 1.0177 | 0.2864 | 0.0000 | 0.2322 | 0.0133 | 0.2208 |
| MEOX1 | 0.0000 | 0.0536 | 0.1642 | 0.0438 | 0.9639 | 0.0000 |
| MIF | 0.4348 | 0.3316 | 0.9576 | 0.4402 | 0.0008 | 0.6845 |
| MIR99AHG | 0.0371 | 0.2791 | 0.3859 | 0.4466 | 1.7947 | 0.2232 |
| MME | 0.0009 | 0.0000 | 0.0640 | 0.4532 | 0.0419 | 0.5791 |
| MRAP2 | 0.0430 | 0.7825 | 0.0000 | 0.2177 | 0.2314 | 0.0000 |
| MRPL24 | 0.1643 | 1.1324 | 0.2156 | 0.1207 | 0.2213 | 0.1778 |
| MTRNR2L1 | 0.2795 | 0.5589 | 0.4897 | 0.0719 | 0.5523 | 0.0000 |
| NACC2 | 0.5312 | 0.0000 | 0.7176 | 0.2474 | 0.0000 | 0.1055 |
| NAMPT | 0.3355 | 0.0000 | 0.0493 | 0.7543 | 0.3154 | 0.3500 |
| NCAPD2 | 1.3843 | 0.4110 | 0.1605 | 0.1233 | 0.2041 | 0.3231 |

| | | | | | | |
|---|---|---|---|---|---|---|
| NCAPG | 1.6056 | 0.4449 | 0.0000 | 0.0000 | 0.0000 | 0.5243 |
| NELFE | 0.9382 | 0.2255 | 0.5894 | 0.8561 | 0.3602 | 0.0798 |
| NEURL2 | 0.6888 | 0.1217 | 0.0000 | 0.2556 | 0.7216 | 0.4336 |
| NFIA | 0.1194 | 0.8389 | 0.0000 | 0.3854 | 1.5045 | 0.2708 |
| NFIX | 0.0000 | 0.8819 | 0.1383 | 0.0000 | 1.3919 | 0.7968 |
| NMB | 0.2126 | 0.1909 | 0.6634 | 0.7944 | 0.0000 | 0.3640 |
| NPM1 | 0.0000 | 1.0465 | 0.0000 | 0.0029 | 0.0826 | 0.0446 |
| NR0B2 | 0.0000 | 0.8362 | 0.0000 | 0.0000 | 0.1422 | 0.0000 |
| NRP2 | 0.1462 | 0.0000 | 0.4996 | 0.0000 | 0.0000 | 0.0534 |
| NUP155 | 1.1296 | 0.4140 | 0.0620 | 0.3285 | 0.2288 | 0.4554 |
| OAZ1 | 0.8583 | 0.5931 | 0.6573 | 1.1219 | 0.5151 | 0.5871 |
| ORC1 | 0.9777 | 0.3231 | 0.1638 | 0.9547 | 0.1157 | 0.0101 |
| P2RY2 | 0.1789 | 0.0331 | 0.7738 | 0.2163 | 0.0000 | 0.5005 |
| P2RY8 | 0.2334 | 0.0728 | 0.0000 | 0.2788 | 1.6555 | 0.0000 |
| P4HA1 | 0.0430 | 0.1009 | 0.4121 | 0.8384 | 0.0000 | 0.5460 |
| P4HA2 | 0.3225 | 0.1659 | 0.1245 | 0.5449 | 0.1088 | 0.7371 |
| PAX8 | 0.7680 | 0.0000 | 0.5631 | 0.0000 | 0.0000 | 0.0000 |
| PAX8-AS1 | 0.5656 | 0.0447 | 0.3435 | 0.0750 | 0.0071 | 0.0000 |
| PBXIP1 | 0.0000 | 0.5144 | 0.4130 | 0.0000 | 0.4392 | 0.1667 |
| PCDH20 | 0.0000 | 0.4318 | 0.0000 | 0.1465 | 0.0000 | 0.0000 |
| PCF11 | 0.2613 | 0.9351 | 0.2527 | 0.0950 | 1.1086 | 0.4077 |
| PCOLCE2 | 0.0000 | 0.0076 | 0.1188 | 0.5379 | 0.0000 | 0.0542 |
| PDLIM7 | 0.1954 | 0.0000 | 0.4086 | 0.3731 | 0.1144 | 0.6779 |
| PEX11B | 0.1066 | 1.3518 | 0.0000 | 0.5264 | 0.2883 | 0.2455 |
| PFKFB4 | 0.5485 | 0.2199 | 0.6769 | 0.4272 | 0.1428 | 0.2854 |
| PGAM5 | 0.9213 | 0.0000 | 0.3859 | 0.4866 | 0.0000 | 0.0000 |
| PGBD3 | 0.6174 | 0.3626 | 0.4335 | 0.2008 | 0.5630 | 0.7384 |
| PHACTR3 | 0.1489 | 0.0000 | 0.3225 | 0.1416 | 0.0026 | 0.0728 |
| PHLDA1 | 0.0838 | 0.1387 | 0.7170 | 0.1250 | 0.6249 | 1.5017 |
| PHOSPHO2 | 0.3445 | 1.0681 | 0.0000 | 0.4652 | 0.4054 | 0.0514 |
| PIGL | 1.0637 | 0.1481 | 0.5587 | 0.3049 | 0.2423 | 0.0000 |
| PLAC9 | 0.0707 | 0.0000 | 0.0000 | 0.1090 | 1.2901 | 0.0766 |
| PLAU | 0.2139 | 0.0000 | 0.2764 | 0.0000 | 0.0249 | 0.8793 |
| PLEKHS1 | 0.0000 | 0.6411 | 0.3407 | 0.0862 | 0.2791 | 0.0176 |
| PLIN2 | 0.3057 | 0.0000 | 0.0818 | 1.0167 | 0.4683 | 0.2095 |
| PLIN3 | 0.3365 | 0.2607 | 0.9673 | 0.9320 | 0.1395 | 0.4103 |
| PLOD1 | 0.0595 | 0.0000 | 1.2074 | 0.7504 | 0.3668 | 0.8026 |
| PLOD2 | 0.1489 | 0.0922 | 0.2366 | 0.2919 | 0.1729 | 0.8899 |
| POC1A | 1.3753 | 0.3309 | 0.3179 | 0.4709 | 0.0000 | 0.0000 |
| POLA2 | 0.8413 | 0.2234 | 0.3296 | 0.1331 | 0.2137 | 0.0000 |
| POP5 | 0.5635 | 0.5070 | 1.5160 | 0.2263 | 0.1092 | 0.1799 |
| POU2AF1 | 0.0611 | 0.4732 | 0.0000 | 0.0007 | 0.9240 | 0.0000 |
| PP7080 | 0.1047 | 0.9680 | 0.0000 | 0.0371 | 0.0000 | 0.0000 |
| PPAPDC1A | 0.0000 | 0.0000 | 0.0000 | 0.7582 | 0.0000 | 1.2230 |

| | | | | | | |
|---|---|---|---|---|---|---|
| PPM1H | 0.0000 | 0.8512 | 0.4600 | 0.2700 | 0.2363 | 0.0000 |
| PPP1R12B | 0.1652 | 0.3193 | 0.7825 | 0.6308 | 0.0253 | 0.4910 |
| PPP1R14B | 0.3673 | 0.2586 | 0.7846 | 0.0000 | 0.3651 | 0.5928 |
| PPP1R3C | 0.0000 | 0.0160 | 0.1325 | 0.3710 | 0.0256 | 0.2554 |
| PPY | 0.0000 | 0.4957 | 0.0000 | 0.0805 | 1.0771 | 0.0000 |
| PRC1 | 0.9560 | 0.3521 | 0.0407 | 0.0375 | 0.0000 | 0.3200 |
| PRDM16 | 0.0000 | 1.1224 | 0.0000 | 0.0000 | 0.5289 | 0.0867 |
| PREP | 0.0587 | 0.9830 | 0.3047 | 0.1977 | 0.0203 | 0.0000 |
| PRKCDBP | 0.2571 | 0.0000 | 1.0161 | 0.5090 | 0.2613 | 0.5936 |
| PRMT7 | 0.1393 | 1.5003 | 0.4373 | 0.0000 | 0.1793 | 0.2230 |
| PROSER2 | 0.9335 | 0.1760 | 0.4026 | 0.3736 | 0.2680 | 0.3965 |
| PRR11 | 0.8207 | 0.0503 | 0.2272 | 0.0000 | 0.0000 | 0.0934 |
| PTGES | 0.5703 | 0.0160 | 0.5702 | 0.0681 | 0.0000 | 0.5634 |
| PTPN21 | 0.2722 | 0.1714 | 0.3219 | 0.4864 | 0.2674 | 0.8423 |
| PXDN | 0.0000 | 0.0000 | 0.3795 | 0.5917 | 0.3108 | 1.1884 |
| PYGL | 0.0808 | 0.0000 | 0.3079 | 0.3384 | 0.1413 | 0.7445 |
| RAB31 | 0.1110 | 0.0000 | 0.2586 | 0.8745 | 0.7552 | 1.1882 |
| RACGAP1 | 1.3720 | 0.3729 | 0.1382 | 0.1936 | 0.0734 | 0.3348 |
| RALGAPB | 0.9974 | 0.5032 | 0.2879 | 0.7587 | 0.2585 | 0.7977 |
| RAP1GAP | 0.0000 | 1.0067 | 0.4657 | 0.2773 | 0.7542 | 0.0000 |
| RASL11B | 0.0000 | 0.1852 | 0.0682 | 0.2236 | 1.2121 | 0.3095 |
| RAVER2 | 0.1985 | 0.9070 | 0.0534 | 0.0890 | 0.2667 | 0.0577 |
| RBMS2 | 0.6118 | 0.1541 | 0.0000 | 0.4022 | 0.3184 | 0.8946 |
| RERE | 0.0485 | 0.7372 | 0.6212 | 0.0026 | 0.9874 | 0.4207 |
| RERGL | 0.2378 | 0.0000 | 0.0000 | 0.1054 | 1.1842 | 0.0000 |
| RFC5 | 1.0809 | 0.2444 | 0.0000 | 0.5248 | 0.1556 | 0.3147 |
| RFK | 0.0000 | 0.6594 | 0.1169 | 0.0000 | 0.4342 | 0.2100 |
| RFX2 | 0.0000 | 0.2219 | 0.2372 | 0.0000 | 0.4551 | 0.2959 |
| RGS3 | 0.2370 | 0.1243 | 0.0000 | 0.8096 | 0.2269 | 0.3212 |
| RGS5 | 0.0000 | 0.4317 | 0.0455 | 0.0788 | 0.5794 | 0.0934 |
| RHOF | 0.7466 | 0.1749 | 0.4760 | 0.1428 | 0.0000 | 0.5878 |
| RMND5A | 0.2696 | 0.1188 | 0.2601 | 0.7065 | 0.0000 | 0.0750 |
| RNF103 | 0.0344 | 1.2504 | 0.1672 | 0.5545 | 0.2894 | 0.0635 |
| RPA2 | 0.4727 | 0.6964 | 0.7005 | 0.4129 | 1.4239 | 0.2443 |
| RPIA | 0.4609 | 1.3515 | 0.2200 | 0.1918 | 0.4584 | 0.0000 |
| SAMD5 | 0.1340 | 0.5397 | 0.0000 | 0.0000 | 0.0860 | 0.0000 |
| SCGB2A1 | 0.0000 | 0.8288 | 0.0000 | 0.1826 | 0.1547 | 0.0000 |
| SCYL2 | 0.7048 | 0.3901 | 0.0000 | 0.9782 | 0.4060 | 0.9614 |
| SDIM1 | 0.0000 | 0.0455 | 0.2422 | 0.0000 | 0.5017 | 0.0000 |
| SEC23IP | 0.3380 | 1.2955 | 0.0000 | 0.5310 | 0.3578 | 0.4605 |
| SELENBP1 | 0.0000 | 1.2032 | 0.3621 | 0.2011 | 0.2603 | 0.0000 |
| SEPW1 | 0.0349 | 0.9518 | 1.2360 | 0.0000 | 0.6293 | 0.5568 |
| SERPINB3 | 0.0000 | 0.0000 | 0.1755 | 0.1787 | 0.0000 | 0.0506 |
| SERPINH1 | 0.0000 | 0.0115 | 0.3898 | 0.2169 | 0.4300 | 1.0203 |

| | | | | | | |
|---|---|---|---|---|---|---|
| SERTAD2 | 0.2931 | 0.1441 | 0.8991 | 0.9858 | 0.4859 | 0.4437 |
| SGSM1 | 0.0000 | 0.9290 | 0.0817 | 0.0211 | 0.8410 | 0.0000 |
| SH3GL1 | 0.1173 | 0.1075 | 1.0090 | 1.2494 | 0.2155 | 0.0000 |
| SLAMF9 | 0.0435 | 0.0000 | 0.0000 | 0.6663 | 0.0000 | 0.0657 |
| SLC12A2 | 0.0380 | 0.9089 | 0.3449 | 0.0968 | 0.4855 | 0.1821 |
| SLC15A1 | 0.0000 | 0.0000 | 0.4779 | 0.0000 | 0.0569 | 0.0565 |
| SLC16A3 | 0.1282 | 0.3828 | 1.1047 | 0.4222 | 0.0000 | 0.9957 |
| SLC2A1 | 0.1786 | 0.1209 | 0.9980 | 0.4099 | 0.0000 | 0.7045 |
| SLC2A3 | 0.0000 | 0.0000 | 0.3369 | 0.7592 | 0.3268 | 0.7204 |
| SLC30A3 | 0.4502 | 0.5017 | 0.0822 | 0.2136 | 0.6568 | 0.0654 |
| SLC40A1 | 0.0000 | 0.8927 | 0.0000 | 0.5789 | 0.2440 | 0.1550 |
| SMOX | 0.3692 | 0.2900 | 1.4313 | 0.9987 | 0.1840 | 0.0000 |
| SNORA11D | 0.0849 | 0.2729 | 0.4795 | 0.4375 | 0.0039 | 0.2687 |
| SNRPB | 0.9900 | 0.0786 | 0.4143 | 0.9037 | 0.0238 | 0.0000 |
| SOBP | 0.0000 | 0.1979 | 0.8103 | 0.1044 | 1.3581 | 0.0039 |
| SOD2 | 0.5780 | 0.1207 | 0.0000 | 0.4656 | 0.4023 | 0.1652 |
| SPHK1 | 0.2590 | 0.0000 | 0.2748 | 0.0907 | 0.6221 | 1.4095 |
| SPIN4 | 0.8495 | 0.3236 | 0.7960 | 0.3855 | 0.2224 | 0.3985 |
| SPOCD1 | 0.0000 | 0.0000 | 0.1782 | 0.2094 | 0.0000 | 0.7594 |
| SPOCK1 | 0.1196 | 0.0000 | 0.0293 | 0.5189 | 0.3390 | 1.2727 |
| SPP1 | 0.0294 | 0.0805 | 0.0000 | 1.0413 | 0.3073 | 0.7357 |
| ST3GAL2 | 0.3414 | 0.0000 | 0.8015 | 1.0746 | 0.4432 | 0.0000 |
| ST6GAL1 | 0.1717 | 0.8423 | 0.0000 | 0.2289 | 0.6651 | 0.0916 |
| ST6GALNAC1 | 0.0396 | 0.9957 | 0.0803 | 0.1154 | 0.0000 | 0.1050 |
| STAT5B | 0.0000 | 0.9053 | 0.3202 | 0.0618 | 1.3050 | 0.2213 |
| STK39 | 0.1526 | 0.9966 | 0.2351 | 0.1373 | 0.0838 | 0.1226 |
| SUGCT | 0.0000 | 0.0321 | 0.0000 | 0.6297 | 0.1256 | 0.9331 |
| SULF2 | 0.1725 | 0.1513 | 0.4552 | 0.1878 | 0.3858 | 0.7665 |
| SYNE2 | 0.0000 | 0.8824 | 0.2432 | 0.0000 | 0.2767 | 0.2763 |
| TAF5L | 0.2232 | 1.0626 | 0.1753 | 0.2440 | 0.2327 | 0.2249 |
| TARBP2 | 0.6779 | 0.3829 | 1.2178 | 0.6116 | 0.1843 | 0.0000 |
| TCEA3 | 0.0000 | 0.8898 | 0.2645 | 0.0922 | 0.6204 | 0.0000 |
| TCTA | 0.0000 | 0.7508 | 0.8167 | 0.0875 | 0.9836 | 0.0178 |
| TGFBI | 0.1874 | 0.0000 | 0.1522 | 0.1879 | 0.0548 | 0.9986 |
| THSD7B | 0.0859 | 0.2031 | 0.0000 | 0.2900 | 0.9574 | 0.1114 |
| TLE4 | 0.0509 | 0.8787 | 0.0746 | 0.3315 | 0.8984 | 0.4660 |
| TM9SF3 | 0.0000 | 1.0785 | 0.2190 | 0.0000 | 0.1641 | 0.2114 |
| TMED1 | 0.2561 | 0.3378 | 1.1457 | 0.8311 | 0.4929 | 0.2755 |
| TMEM26 | 0.0407 | 0.0237 | 0.1028 | 0.4886 | 0.2223 | 1.4490 |
| TMTC4 | 0.0000 | 1.2865 | 0.3348 | 0.2090 | 0.1995 | 0.2756 |
| TNFRSF10D | 0.1474 | 0.1117 | 0.6603 | 0.4579 | 0.0000 | 0.1751 |
| TNFRSF17 | 0.0258 | 0.0455 | 0.0000 | 0.0803 | 0.5772 | 0.0000 |
| TNFRSF6B | 0.6268 | 0.0000 | 0.0684 | 0.1841 | 0.0000 | 0.3940 |
| TOM1 | 0.0000 | 0.1032 | 1.4892 | 0.8140 | 0.6813 | 0.5236 |

| | | | | | | |
|---|---|---|---|---|---|---|
| TOM1L2 | 0.1892 | 0.0000 | 0.6276 | 0.3305 | 0.0489 | 0.2346 |
| TOR2A | 0.0000 | 0.9859 | 0.4755 | 0.2012 | 0.5273 | 0.0000 |
| TPD52L2 | 0.6311 | 0.1617 | 1.3107 | 0.6501 | 0.4351 | 0.2322 |
| TPX2 | 1.3192 | 0.1540 | 0.0351 | 0.1488 | 0.0392 | 0.1087 |
| TRAPPC2 | 0.5080 | 1.0792 | 0.0000 | 0.4917 | 0.6155 | 0.1418 |
| TREM1 | 0.0472 | 0.0000 | 0.0870 | 0.7055 | 0.0000 | 0.3006 |
| TRERF1 | 0.4920 | 0.2861 | 0.3810 | 0.1345 | 0.0517 | 0.1346 |
| TRIM2 | 0.1310 | 1.1544 | 0.3127 | 0.3092 | 0.3595 | 0.0000 |
| TSTD1 | 0.1685 | 1.2229 | 0.4834 | 0.0685 | 0.4502 | 0.0191 |
| TUBA1C | 1.3100 | 0.5454 | 0.5360 | 0.5305 | 0.2711 | 0.5032 |
| TWIST1 | 0.0000 | 0.0000 | 0.1970 | 0.9070 | 0.1202 | 1.2015 |
| UFC1 | 0.0000 | 1.1861 | 0.2466 | 0.4651 | 0.2997 | 0.0000 |
| UHRF2 | 0.1520 | 0.2931 | 0.3251 | 0.4968 | 0.6565 | 1.1025 |
| UPP1 | 0.5505 | 0.0000 | 0.7864 | 0.4294 | 0.1567 | 0.1100 |
| USP30 | 0.5449 | 0.1353 | 0.3862 | 0.0000 | 0.0771 | 0.0000 |
| VPS35 | 0.3941 | 1.3902 | 0.0000 | 0.5311 | 0.0000 | 0.2457 |
| VSTM2L | 0.3176 | 0.0000 | 0.9398 | 0.0000 | 0.0509 | 0.0656 |
| WNT2B | 0.0885 | 0.1107 | 0.0000 | 0.0139 | 0.4530 | 0.0000 |
| XXYLT1 | 0.2408 | 0.0000 | 1.0488 | 1.0782 | 0.4595 | 0.8654 |
| ZBED2 | 0.1569 | 0.0000 | 0.1800 | 0.0000 | 0.0000 | 0.6435 |
| ZFPM1 | 0.0000 | 1.2172 | 0.2917 | 0.0000 | 0.4340 | 0.1504 |
| ZNF185 | 0.2542 | 0.1747 | 1.0210 | 0.4834 | 0.0000 | 0.7221 |
| ZNF565 | 0.0701 | 0.2851 | 0.0717 | 0.0569 | 0.2393 | 0.0768 |
| ZNF658 | 0.0000 | 0.8769 | 0.0000 | 0.0000 | 0.9099 | 0.2753 |
| ZPLD1 | 0.0000 | 0.0000 | 0.1873 | 0.0325 | 0.0294 | 0.1074 |
| ZSCAN16 | 0.3012 | 1.4502 | 0.0000 | 0.0175 | 0.5146 | 0.5090 |
| ZSCAN32 | 0.3467 | 1.1558 | 0.4982 | 0.3027 | 0.7286 | 0.2378 |

# Appendix B

# MSigDB signatures correlated with axis A1

Table B.1: MSigDB signatures substantially correlated with activity of the prognostic axis A1.

| MSigDB set |
|---|
| c5.M_PHASE/c5.MITOSIS/c5.M_PHASE_OF_MITOTIC_CELL_CYCLE |
| c5.REGULATION_OF_MITOSIS |
| c4.GNF2_RFC3/c4.GNF2_RFC4/c4.GNF2_SMC2L1/c4.GNF2_CKS1B/c4.GNF2_CKS2/c4.GNF2_TT |
| c5.CELL_CYCLE_PROCESS/c5.MITOTIC_CELL_CYCLE/c5.CELL_CYCLE_PHASE |
| c5.SPINDLE |
| c4.MORF_BUB1B |
| c6.CSR_LATE_UP.V1_SIGNED |
| c5.SPINDLE_POLE |
| c2.PID_PLK1_PATHWAY |
| c5.ORGANELLE_PART/c5.INTRACELLULAR_ORGANELLE_PART |
| c2.REACTOME_CELL_CYCLE/c2.REACTOME_CELL_CYCLE_MITOTIC |
| c2.REACTOME_CYCLIN_A_B1_ASSOCIATED_EVENTS_DURING_G2_M_TRANSITION |
| c2.REACTOME_MITOTIC_PROMETAPHASE |
| c2.KEGG_CELL_CYCLE |
| c5.CHROMOSOME_SEGREGATION |
| c4.MORF_FEN1 |
| c2.REACTOME_G1_S_SPECIFIC_TRANSCRIPTION |
| c2.REACTOME_ACTIVATION_OF_THE_PRE_REPLICATIVE_COMPLEX/c2.REACTOME_ACTI |
| c2.REACTOME_E2F_ENABLED_INHIBITION_OF_PRE_REPLICATION_COMPLEX_FORMATIO |
| c2.REACTOME_E2F_MEDIATED_REGULATION_OF_DNA_REPLICATION |
| c5.CELL_CYCLE_GO_0007049 |
| c2.REACTOME_KINESINS |
| c3.V$ELK1_02 |
| c5.SPINDLE_MICROTUBULE |
| c5.MITOTIC_CELL_CYCLE_CHECKPOINT |
| c2.REACTOME_CELL_CYCLE_CHECKPOINTS/c2.REACTOME_G1_S_TRANSITION/c2.REACT |
| c4.MORF_ESPL1 |
| c4.MORF_BUB1 |
| c4.MORF_BUB3/c4.MORF_RAD23A |
| c5.CONDENSED_CHROMOSOME |
| c4.MORF_RFC4/c4.MORF_RRM1 |
| c2.BIOCARTA_G2_PATHWAY |
| c3.SCGGAAGY_V$ELK1_02 |
| c2.PID_AURORA_A_PATHWAY |
| c5.MITOTIC_SISTER_CHROMATID_SEGREGATION/c5.SISTER_CHROMATID_SEGREGATION |
| c4.MORF_UNG |
| c2.PID_FOXM1PATHWAY |
| c4.MORF_GSPT1 |
| c2.REACTOME_METABOLISM_OF_NUCLEOTIDES |
| c2.PID_ATR_PATHWAY |
| c2.BIOCARTA_MCM_PATHWAY |
| c4.MORF_CCNF |
| c5.CELL_CYCLE_CHECKPOINT_GO_0000075 |
| c5.MITOTIC_SPINDLE_ORGANIZATION_AND_BIOGENESIS/c5.SPINDLE_ORGANIZATION_AN |
| c4.MORF_EI24 |
| c5.DOUBLE_STRAND_BREAK_REPAIR |
| c4.GNF2_PA2G4/c4.GNF2_RAN |
| c2.REACTOME_G2_M_DNA_DAMAGE_CHECKPOINT |
| c2.KEGG_PYRIMIDINE_METABOLISM |

# Appendix C

# MSigDB signatures correlated with axis A2

Table C.1: MSigDB signatures substantially correlated with activity of the prognostic axis A2.

| GeneSet |
|---|
| c2.PID_INTEGRIN1_PATHWAY |
| c2.PID_INTEGRIN3_PATHWAY |
| c2.PID_UPA_UPAR_PATHWAY |
| c4.GNF2_PTX3 |
| c2.KEGG_ECM_RECEPTOR_INTERACTION |
| c2.PID_INTEGRIN5_PATHWAY |
| c4.GNF2_MMP1 |
| c2.REACTOME_EXTRACELLULAR_MATRIX_ORGANIZATION/c2.REACTOME_COLLAGEN_F |
| c5.AXON_GUIDANCE |
| c2.KEGG_FOCAL_ADHESION |
| c2.PID_SYNDECAN_1_PATHWAY |
| c2.REACTOME_CELL_EXTRACELLULAR_MATRIX_INTERACTIONS |
| c2.PID_INTEGRIN_CS_PATHWAY |
| c5.TISSUE_DEVELOPMENT |
| c5.COLLAGEN |
| c6.CORDENONSI_YAP_CONSERVED_SIGNATURE |
| c6.LEF1_UP.V1_SIGNED |
| c2.REACTOME_INTEGRIN_CELL_SURFACE_INTERACTIONS |
| c5.AXONOGENESIS/c5.CELLULAR_MORPHOGENESIS_DURING_DIFFERENTIATION |
| c6.STK33_NOMO_SIGNED |
| c7.GSE17721_CTRL_VS_CPG_12H_BMDM_SIGNED |
| c7.GSE1460_INTRATHYMIC_T_PROGENITOR_VS_THYMIC_STROMAL_CELL_SIGNED |

# Appendix D

# Approximate calculation of PARSE scores

Exact calculation of PARSE score requires the solution of a number of NNLS problems, which complicates application. The NNLS solutions can be approximated with conventional least squares solutions, ultimately transforming the calculation of an approximate PARSE score into a simple weighted sum of gene expression measurements.

Recall that NMF finds factorizations of the form $A = WH$, with all elements of $A$, $W$, and $H$, being non-negative. In the reverse problem of PARSE calculation, $A$ and $\widehat{W}$ are supplied, and $H$ is to be estimated. I propose an approximation that removes the requirement that $H$ be non-negative, $H \approx \widehat{W}^{+}A$, where $\widehat{W}^{+}$ is the Moore-Penrose pseudoinverse of $\widehat{W}$. By combining this approximation with the linear combination of metagene coefficients that forms the PARSE score, we can approximate PARSE as a simple weighted sum of gene expression measurements:

$$P = LH \tag{D.1}$$

$$\approx L\widehat{W}^{+}A \tag{D.2}$$

$$= kA \tag{D.3}$$

where $P$ is the vector of PARSE score values, $L$ is the metagene loadings for the PARSE score, $L = \begin{pmatrix} 1.354 & -1.548 & 0 & 0 & -1.354 & 1.548 \end{pmatrix}$, and $k$ is a row vector of gene loadings for calculation of an approximate PARSE score. Approximation of $P$ by $kA$ appears excellent; when tested on APGI gene expression measurements, the approximation closely matched the more laborious exact NNLS solution (Figure D.1).

To use the approximation in practice, perform the following steps:

1. Prepare a gene $\times$ sample matrix of linear expression estimates $A$, in which values for each row (gene) have been scaled to encompass the range 0 to 1.

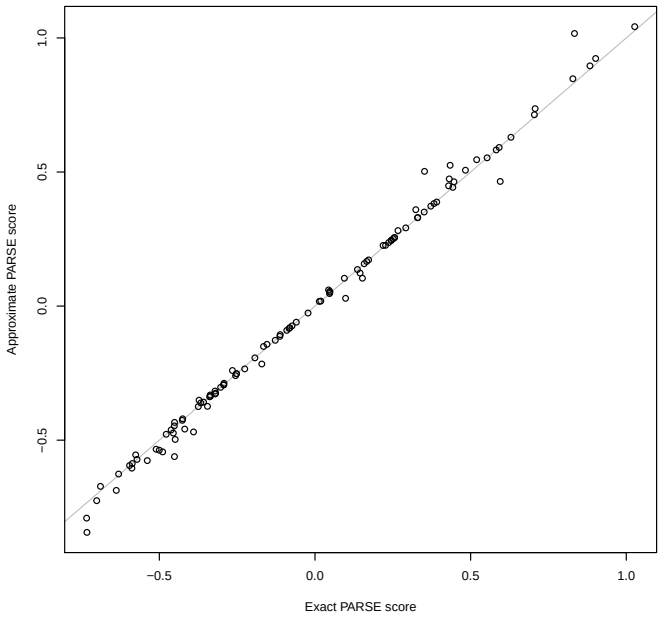


Figure D.1: The linear PARSE score approximation $P \approx kA$ closely matches the exact version calculated using NNLS, when evaluated on APGI GEX data.

2. Subset $A$ to only the genes present in the $k$ table (below), and arrange rows of $A$ so that they exactly match the order of rows of $k$. If genes present in $k$ are missing from $A$, insert all-zero rows for these genes into $A$.

3. Calculate approximate PARSE scores $P$ as $P = kA$. This is equivalent to, for each column (sample) of $A$, multiplying each entry of the column of $A$ with the corresponding entry of $k$, and summing the results.

The loading vector for the calculation of approximate PARSE score, $k^T$, follows.

| | Value |
|---|---|
| A4GALT | 0.00418 |
| A4GNT | -0.01632 |
| ABHD16A | 0.00143 |
| ABHD5 | 0.01227 |
| ABLIM1 | -0.01392 |
| ACE | -0.00556 |
| ACKR3 | 0.00802 |
| ACYP2 | -0.01298 |

| | |
|---|---|
| ADH1A | -0.01845 |
| ADM | 0.00122 |
| AGRP | -0.00509 |
| AKIP1 | 0.00545 |
| AKR1A1 | -0.01321 |
| ALDH5A1 | -0.02452 |
| ALOX5AP | -0.00179 |
| AMOT | -0.00825 |
| ANGPTL2 | 0.01178 |
| ANGPTL4 | 0.01365 |
| ANKLE2 | 0.01205 |
| ANKRD22 | -0.00941 |
| ANKRD37 | 0.00474 |
| ANLN | 0.04364 |
| APCDD1 | 0.01244 |
| APCS | 0.00602 |
| ARFGAP3 | -0.01070 |
| ARHGAP24 | -0.02524 |
| ARHGEF19 | -0.00476 |
| ARL4C | 0.02609 |
| ARSD | -0.01466 |
| ASPM | 0.01593 |
| ATAD2 | 0.02602 |
| ATF7IP2 | -0.00405 |
| ATL3 | 0.00972 |
| AURKB | 0.01869 |
| AXIN2 | -0.01658 |
| B3GALTL | 0.01113 |
| BAMBI | -0.00680 |
| BBS2 | 0.00587 |
| BCKDK | -0.02452 |
| BCL11B | -0.02161 |
| BIRC5 | 0.02419 |
| BOC | -0.03047 |
| BTN3A1 | -0.00868 |
| C1orf56 | -0.00865 |
| C1QTNF6 | 0.01572 |
| C2orf70 | -0.01360 |
| C5orf46 | 0.01559 |
| C9orf152 | -0.02152 |
| CA8 | -0.01129 |
| CACHD1 | -0.01313 |
| CADPS2 | -0.02136 |
| CAMK1G | -0.01790 |

| | |
|---|---|
| CAPN6 | -0.02615 |
| CARHSP1 | -0.01515 |
| CATSPER1 | 0.00163 |
| CAV1 | 0.02989 |
| CCDC88A | 0.01480 |
| CCL19 | -0.01715 |
| CCNB1 | 0.03071 |
| CCR7 | -0.01775 |
| CD70 | 0.00954 |
| CDA | 0.02792 |
| CDC45 | 0.01256 |
| CDK12 | -0.01624 |
| CDK2 | 0.01546 |
| CEBPB | 0.00404 |
| CEP55 | 0.03755 |
| CFDP1 | -0.00617 |
| CHAF1B | 0.00920 |
| CHEK1 | 0.03669 |
| CHN2 | -0.02051 |
| CIDEC | -0.00596 |
| CIDECP | -0.00684 |
| CKAP2L | 0.03545 |
| CLEC3B | -0.01500 |
| CNIH3 | 0.01413 |
| CNNM1 | -0.01611 |
| COL12A1 | 0.04098 |
| COL5A3 | 0.03177 |
| COL7A1 | 0.01688 |
| COLGALT1 | 0.02272 |
| COLGALT2 | -0.00903 |
| COX4I2 | -0.00943 |
| CSNK1D | -0.01128 |
| CST6 | 0.02032 |
| CTSL | -0.01263 |
| CTSV | 0.00987 |
| CYP2S1 | -0.01044 |
| DCAF8 | -0.02374 |
| DCBLD2 | 0.03351 |
| DCUN1D5 | 0.02056 |
| DENND1A | 0.01898 |
| DERA | 0.01568 |
| DHRS9 | -0.00454 |
| DKK1 | 0.00649 |
| DNAJC9 | 0.01385 |

| | |
|---|---|
| DPY19L1 | 0.00749 |
| DSG2 | 0.01463 |
| DSG3 | 0.02070 |
| DYNC2H1 | -0.01537 |
| E2F7 | 0.03923 |
| EDIL3 | 0.01326 |
| EIF2AK3 | -0.02073 |
| ELMOD3 | -0.03300 |
| EMP3 | 0.01550 |
| ENO2 | 0.02998 |
| EPHX2 | -0.02392 |
| ERRFI1 | 0.01597 |
| EXOSC8 | -0.00850 |
| EYA3 | 0.02671 |
| FAH | 0.01035 |
| FAM120AOS | -0.00980 |
| FAM134B | -0.01945 |
| FAM189A2 | -0.01692 |
| FAM83A | 0.01202 |
| FAM91A1 | 0.01341 |
| FBXO22 | 0.00649 |
| FBXW8 | -0.00891 |
| FEM1B | 0.04785 |
| FER | 0.02675 |
| FGB | -0.00252 |
| FGD6 | 0.02545 |
| FGG | 0.00548 |
| FHDC1 | -0.01380 |
| FLRT3 | 0.01416 |
| FRZB | -0.03715 |
| FSCN1 | 0.02159 |
| FST | 0.01504 |
| FYN | -0.01133 |
| GAB2 | -0.03742 |
| GABPB1 | 0.01929 |
| GAPDH | 0.02073 |
| GATA6 | -0.01780 |
| GATC | 0.02661 |
| GIMAP2 | -0.03176 |
| GINS2 | 0.01713 |
| GNPAT | -0.01458 |
| GOLM1 | -0.01171 |
| GPC3 | -0.02419 |
| GPR176 | 0.00563 |

| | |
|---|---|
| HIPK2 | -0.02620 |
| HJURP | 0.02296 |
| HRASLS2 | 0.00196 |
| HSP90B1 | -0.00641 |
| HSPB6 | -0.01586 |
| ICAM2 | -0.00232 |
| IDH2 | 0.00528 |
| IFT140 | -0.02068 |
| IGFBP1 | 0.00427 |
| IGLL3P | -0.01241 |
| IKBIP | -0.00033 |
| IL1R2 | -0.00660 |
| IL20RB | 0.02671 |
| IL33 | -0.00991 |
| ITGA5 | 0.01407 |
| ITPKB | -0.01390 |
| KANK4 | 0.03261 |
| KCNQ3 | 0.00040 |
| KCTD10 | 0.01501 |
| KCTD5 | -0.01440 |
| KIAA0513 | -0.02989 |
| KIAA1549L | 0.01354 |
| KIF14 | 0.01477 |
| KIF20A | 0.02967 |
| KIF2C | 0.01417 |
| KLHL5 | 0.02641 |
| KNTC1 | 0.02375 |
| KRT17 | 0.01644 |
| KRT6A | 0.01795 |
| KRT6C | 0.00798 |
| KRT7 | 0.01916 |
| KYNU | 0.01181 |
| LAMA5 | 0.00174 |
| LCNL1 | -0.01571 |
| LDHA | 0.04004 |
| LETM2 | 0.01687 |
| LGALS9B | -0.00232 |
| LINC01184 | -0.01837 |
| LMO3 | -0.02246 |
| LMTK2 | 0.00804 |
| LOC100506562 | -0.00290 |
| LOX | 0.02695 |
| LYNX1 | 0.00001 |
| MAP3K8 | 0.00338 |

| | |
|---|---|
| MARCKSL1 | -0.00884 |
| MARS2 | -0.01442 |
| MC1R | -0.02281 |
| MCEMP1 | 0.00025 |
| MCM10 | 0.02451 |
| MCM4 | 0.02708 |
| MCOLN2 | -0.01684 |
| MELK | 0.02067 |
| MEOX1 | -0.01961 |
| MIF | 0.01560 |
| MIR99AHG | -0.03712 |
| MME | 0.01102 |
| MRAP2 | -0.01810 |
| MRPL24 | -0.01395 |
| MTRNR2L1 | -0.01563 |
| NACC2 | 0.00733 |
| NAMPT | 0.00071 |
| NCAPD2 | 0.02756 |
| NCAPG | 0.04487 |
| NELFE | -0.00390 |
| NEURL2 | 0.01012 |
| NFIA | -0.03387 |
| NFIX | -0.01186 |
| NMB | -0.00205 |
| NPM1 | -0.01520 |
| NR0B2 | -0.01468 |
| NRP2 | 0.00250 |
| NUP155 | 0.02330 |
| OAZ1 | -0.00134 |
| ORC1 | -0.00199 |
| P2RY2 | 0.01288 |
| P2RY8 | -0.03043 |
| P4HA1 | 0.00225 |
| P4HA2 | 0.01770 |
| PAX8 | 0.01350 |
| PAX8-AS1 | 0.00830 |
| PBXIP1 | -0.01174 |
| PCDH20 | -0.00861 |
| PCF11 | -0.01710 |
| PCOLCE2 | -0.00752 |
| PDLIM7 | 0.01678 |
| PEX11B | -0.02280 |
| PFKFB4 | 0.00525 |
| PGAM5 | 0.00973 |

| | |
|---|---|
| PGBD3 | 0.01700 |
| PHACTR3 | 0.00172 |
| PHLDA1 | 0.03330 |
| PHOSPHO2 | -0.02129 |
| PIGL | 0.00833 |
| PLAC9 | -0.02093 |
| PLAU | 0.03213 |
| PLEKHS1 | -0.01672 |
| PLIN2 | -0.01174 |
| PLIN3 | -0.00506 |
| PLOD1 | 0.00369 |
| PLOD2 | 0.02261 |
| POC1A | 0.01507 |
| POLA2 | 0.00692 |
| POP5 | -0.00224 |
| POU2AF1 | -0.02222 |
| PP7080 | -0.01242 |
| PPAPDC1A | 0.02867 |
| PPM1H | -0.02311 |
| PPP1R12B | 0.00096 |
| PPP1R14B | 0.01352 |
| PPP1R3C | 0.00125 |
| PPY | -0.02787 |
| PRC1 | 0.02492 |
| PRDM16 | -0.02289 |
| PREP | -0.01799 |
| PRKCDBP | 0.00755 |
| PRMT7 | -0.01665 |
| PROSER2 | 0.01761 |
| PRR11 | 0.01859 |
| PTGES | 0.02681 |
| PTPN21 | 0.01723 |
| PXDN | 0.02281 |
| PYGL | 0.01714 |
| RAB31 | 0.01316 |
| RACGAP1 | 0.02957 |
| RALGAPB | 0.02214 |
| RAP1GAP | -0.03483 |
| RASL11B | -0.01808 |
| RAVER2 | -0.01352 |
| RBMS2 | 0.02834 |
| RERE | -0.01635 |
| RERGL | -0.01801 |
| RFC5 | 0.01848 |

| | |
|---|---|
| RFK | -0.01090 |
| RFX2 | -0.00264 |
| RGS3 | -0.00319 |
| RGS5 | -0.01505 |
| RHOF | 0.02828 |
| RMND5A | -0.00614 |
| RNF103 | -0.03019 |
| RPA2 | -0.02756 |
| RPIA | -0.02226 |
| SAMD5 | -0.00655 |
| SCGB2A1 | -0.01773 |
| SCYL2 | 0.01826 |
| SDIM1 | -0.01083 |
| SEC23IP | -0.01125 |
| SELENBP1 | -0.02707 |
| SEPW1 | -0.01161 |
| SERPINB3 | -0.00201 |
| SERPINH1 | 0.02086 |
| SERTAD2 | -0.00995 |
| SGSM1 | -0.02933 |
| SH3GL1 | -0.02784 |
| SLAMF9 | -0.00761 |
| SLC12A2 | -0.01821 |
| SLC15A1 | -0.00139 |
| SLC16A3 | 0.01842 |
| SLC2A1 | 0.01424 |
| SLC2A3 | 0.00438 |
| SLC30A3 | -0.01126 |
| SLC40A1 | -0.02146 |
| SMOX | -0.02258 |
| SNORA11D | -0.00256 |
| SNRPB | 0.00276 |
| SOBP | -0.03269 |
| SOD2 | 0.00120 |
| SPHK1 | 0.03861 |
| SPIN4 | 0.01254 |
| SPOCD1 | 0.02117 |
| SPOCK1 | 0.03046 |
| SPP1 | 0.00175 |
| ST3GAL2 | -0.02187 |
| ST6GAL1 | -0.02118 |
| ST6GALNAC1 | -0.01232 |
| STAT5B | -0.03172 |
| STK39 | -0.01196 |

| | |
|---|---|
| SUGCT | 0.01833 |
| SULF2 | 0.01494 |
| SYNE2 | -0.00968 |
| TAF5L | -0.01213 |
| TARBP2 | -0.01019 |
| TCEA3 | -0.02679 |
| TCTA | -0.03326 |
| TGFBI | 0.03259 |
| THSD7B | -0.01931 |
| TLE4 | -0.01794 |
| TM9SF3 | -0.01255 |
| TMED1 | -0.01796 |
| TMEM26 | 0.03659 |
| TMTC4 | -0.01797 |
| TNFRSF10D | -0.00315 |
| TNFRSF17 | -0.01180 |
| TNFRSF6B | 0.02308 |
| TOM1 | -0.01640 |
| TOM1L2 | 0.00266 |
| TOR2A | -0.02926 |
| TPD52L2 | -0.00579 |
| TPX2 | 0.02590 |
| TRAPPC2 | -0.01920 |
| TREM1 | -0.00073 |
| TRERF1 | 0.00581 |
| TRIM2 | -0.02689 |
| TSTD1 | -0.02503 |
| TUBA1C | 0.02053 |
| TWIST1 | 0.02246 |
| UFC1 | -0.03123 |
| UHRF2 | 0.01445 |
| UPP1 | 0.00182 |
| USP30 | 0.00629 |
| VPS35 | -0.01219 |
| VSTM2L | 0.00352 |
| WNT2B | -0.00812 |
| XXYLT1 | 0.00341 |
| ZBED2 | 0.02396 |
| ZFPM1 | -0.02180 |
| ZNF185 | 0.01435 |
| ZNF565 | -0.00565 |
| ZNF658 | -0.01988 |
| ZPLD1 | 0.00165 |
| ZSCAN16 | -0.00720 |

| | |
|---|---|
| ZSCAN32 | -0.02184 |

# Glossary

**APGI** Australian Pancreatic Cancer Genome Initiative. iii, 1, 6–8, 10, 15, 17–19, 21, 23, 25–29, 43, 44

**CPSS** complementary pair subset selection. 7, 23–25

**CPV** clinico-pathological variable. iii, 6, 20, 23, 27, 28

**CV** cross-validation. 8

**DSD** disease-specific death. 7, 24

**DSS** disease-specific survival. ii, 14, 23

**ECM** extracellular matrix. 20

**EMT** epithelial to mesenchymal transition. 18, 21, 22

**FAST** feature aberration at survival times. 7, 23–25

**FDR** false-discovery rate. 7, 24

**FWER** familywise error rate. 9, 16

**GEO** Gene Expression Omnibus. 26

**GEX** gene expression. ii, 1–7, 23, 25, 27, 44

**GSVA** gene set variation analysis. 21, 26–28

**ICA** independent component analysis. 4

**ICGC** International Cancer Genome Consortium. 29

**IDAT** Illumina data. 22, 29

**LASSO** least absolute shrinkage and selection operator. ii, 8, 14

**MDS** multidimensional scaling. 23

**MSigDB** molecular signatures database. i, iii, 2, 19–21, 26–29, 40–42

**NCBI** National Center for Biotechnology Information. 26

**NMF** non-negative matrix factorization. ii, 4, 6, 7, 24, 43

**NNLS** non-negative least squares. 8, 25, 43, 44

**PARSE** prognostic axis risk stratification estimate. i–iii, 8, 9, 16–19, 26, 43, 44

**PCA** principal component analysis. 4

**PDAC** pancreatic ductal adenocarcinoma. 1, 2, 5–7, 9, 10, 18, 23, 26

**SIS** sure independence screening. 7, 23–25

**SNMF/L** sparse non-negative matrix factorization, long variant. ii, 7, 11, 13, 24, 25

**TCGA** The Cancer Genome Atlas. iii, 9, 16–18, 26

**VST** variance stabilizing transform. 23, 24, 27

# References


[1] O. Alter, P. O. Brown, and D. Botstein. Singular value decomposition for genome-wide expression data processing and modeling. *Proceedings of the National Academy of Sciences*, 97(18):10101–10106, August 2000.

[2] Andrew V Biankin, Nicola Waddell, Karin S Kassahn, Marie-Claude Gingras, Lakshmi B Muthuswamy, Amber L Johns, David K Miller, Peter J Wilson, Ann-Marie Patch, Jianmin Wu, and Others. Pancreatic cancer genomes reveal aberrations in axon guidance pathway genes. *Nature*, 491(7424):399–405, 2012.

[3] Jean-Philippe Brunet, Pablo Tamayo, Todd R Golub, and Jill P Mesirov. Metagenes and molecular pattern discovery using matrix factorization. *Proceedings of the National Academy of Sciences of the United States of America*, 101(12):4164–9, March 2004.

[4] Eric A Collisson, Anguraj Sadanandam, Peter Olson, William J Gibb, Morgan Truitt, Shenda Gu, Janine Cooc, Jennifer Weinkle, Grace E Kim, Lakshmi Jakkula, Heidi S Feiler, Andrew H Ko, Adam B Olshen, Kathleen L Danenberg, Margaret A Tempero, Paul T Spellman, Douglas Hanahan, and Joe W Gray. Subtypes of pancreatic ductal adenocarcinoma and their differing responses to therapy. *Nature medicine*, 17(4):500–3, April 2011.

[5] Attila Frigyesi and Mattias Höglund. Non-negative matrix factorization for the analysis of complex gene expression data: identification of clinically relevant tumor subtypes. *Cancer informatics*, (2003), 2008.

[6] Anders Gorst-Rasmussen and Thomas Scheike. Independent screening for single-index hazard rate models with ultrahigh dimensional features. *Journal of the Royal Statistical Society: Series B (Statistical Methodology)*, 75(2):217–245, March 2013.

[7] Christian J Gröger, Markus Grubinger, Thomas Waldhör, Klemens Vierlinger, and Wolfgang Mikulits. Meta-analysis of gene expression signatures defining the epithelial to mesenchymal transition during cancer progression. *PloS one*, 7(12):e51136, January 2012.

[8] Douglas Hanahan and Robert a Weinberg. Hallmarks of cancer: the next generation. *Cell*, 144(5):646–74, March 2011.

[9] Sonja Hänzelmann, Robert Castelo, and Justin Guinney. GSVA: gene set variation analysis for microarray and RNA-Seq data. *BMC bioinformatics*, 14(1):7, January 2013.

[10] H C Harsha, Kumaran Kandasamy, Prathibha Ranganathan, Sandhya Rani, Subhashri Ramabadran, Sashikanth Gollapudi, Lavanya Balakrishnan, Sutopa B Dwivedi, Deepthi Telikicherla, Lakshmi Dhevi N Selvan, Renu Goel, Suresh Mathivanan, Arivusudar Marimuthu, Manoj Kashyap, Robert F Vizza, Robert J Mayer, James a Decaprio, Sudhir Srivastava, Samir M Hanash, Ralph H Hruban, and Akhilesh Pandey. A compendium of potential biomarkers of pancreatic cancer. *PLoS medicine*, 6(4):e1000046, April 2009.

[11] Sture Holm. A simple sequentially rejective multiple test procedure. *Scandinavian journal of statistics*, 6(2):65–70, 1979.

[12] Hyunsoo Kim and Haesun Park. Sparse non-negative matrix factorizations via alternating non-negativity-constrained least squares for microarray data analysis. *Bioinformatics*, 23(12):1495–502, June 2007.

[13] Su-In Lee and Serafim Batzoglou. Application of independent component analysis to microarrays. *Genome biology*, 4(11):R76, January 2003.

[14] Su-In Lee and Serafim Batzoglou. Application of independent component analysis to microarrays. *Genome biology*, 4(11):R76, January 2003.

[15] Michael S. Lewicki and Terrence J. Sejnowski. Learning Overcomplete Representations. *Neural Computation*, 12(2):337–365, February 2000.

[16] Robert C MacCallum, Keith F Widaman, Shaobo Zhang, and Sehee Hong. Sample size in factor analysis. *Psychological Methods*, 4(1):84–99, 1999.

[17] Daruka Mahadevan and Daniel D Von Hoff. Tumor-stroma interactions in pancreatic ductal adenocarcinoma. *Molecular cancer therapeutics*, 6(4):1186–97, April 2007.

[18] Bisakha Ray, Mikael Henaff, Sisi Ma, Efstratios Efstathiadis, Eric R Peskin, Marco Picone, Tito Poli, Constantin F Aliferis, and Alexander Statnikov. Information content and analysis methods for multi-modal high-throughput biomedical data. *Scientific reports*, 4:4411, January 2014.

[19] Samir a Saidi, Cathrine M Holland, David P Kreil, David J C MacKay, D Stephen Charnock-Jones, Cristin G Print, and Stephen K Smith. Independent component analysis of microarray data in the study of endometrial cancer. *Oncogene*, 23(39):6677–83, August 2004.

[20] Rajen D. Shah and Richard J. Samworth. Variable selection with error control: another look at stability selection. *Journal of the Royal Statistical Society B*, 75(1):55–80, January 2013.

[21] Sarah Song, Katia Nones, David Miller, Ivon Harliwong, Karin S Kassahn, Mark Pinese, Marina Pajic, Anthony J Gill, Amber L Johns, Matthew Anderson, and Others. qpure: A tool to estimate tumor cellularity from genome-wide single-nucleotide polymorphism profiles. *PloS one*, 7(9):e45835, 2012.

[22] Jeran K Stratford, David J Bentrem, Judy M Anderson, Cheng Fan, Keith a Volmar, J S Marron, Elizabeth D Routh, Laura S Caskey, Jonathan C Samuel, Channing J Der, Leigh B Thorne, Benjamin F Calvo, Hong Jin Kim, Mark S Talamonti, Christine a Iacobuzio-Donahue, Michael a Hollingsworth, Charles M Perou, and Jen Jen Yeh. A six-gene signature predicts survival of patients with localized pancreatic ductal adenocarcinoma. *PLoS medicine*, 7(7):e1000307, July 2010.

[23] Aravind Subramanian, Pablo Tamayo, Vamsi K. Mootha, Sayan Mukherjee, Benjamin L. Ebert, Michael A. Gillette, Amanda Paulovich, Scott L. Pomeroy, Todd R. Golub, Eric S. Lander, and Jill P. Mesirov. Gene set enrichment analysis: A knowledge-based approach for interpreting genome-wide expression profiles. *Proceedings of the National Academy of Sciences*, 102(43):15545–15550, 2005.

[24] Andrew E Teschendorff, Michel Journée, Pierre a Absil, Rodolphe Sepulchre, and Carlos Caldas. Elucidating the altered transcriptional programs in breast cancer using independent component analysis. *PLoS computational biology*, 3(8):e161, August 2007.

[25] David Venet, Jacques E Dumont, and Vincent Detours. Most random gene expression signatures are significantly associated with breast cancer outcome. *PLoS computational biology*, 7(10):e1002240, October 2011.

[26] Geng Zhang, Peijun He, Hanson Tan, Anuradha Budhu, Jochen Gaedcke, B Michael Ghadimi, Thomas Ried, Harris G Yfantis, Dong H Lee, Anirban Maitra, Nader Hanna, H Richard Alexander, and S Perwez Hussain. Integration of metabolomics and transcriptomics revealed a fatty acid network exerting growth inhibitory effects in human pancreatic cancer. *Clinical cancer research : an official journal of the American Association for Cancer Research*, 19(18):4983–93, September 2013.